Vortices in squeezed Bose-Bose quantum droplets

Poparić, Ivan

University of Split
Faculty of Science

Vortices in squeezed Bose-Bose quantum droplets

Master thesis

Ivan Poparić

Split, September 2024

Temeljna dokumentacijska kartica

Sveučilište u Splitu
Prirodoslovno–matematički fakultet
Odjel za fiziku
Ruđera Boškovića 33, 21000 Split, Hrvatska

Diplomski rad

Vrtlozi u stisnutim Bose-Bose kvantnim kapljicama

Ivan Poparić

Sveučilišni diplomski studij Fizika; smjer: Računarska fizika

Sažetak:

Ovaj rad istražuje svojstva kvantnih kapljica sastavljenih od dvaju hiperfinih stanja kalija-39, stisnutih duž jedne osi, s naglaskom na vrtloge unutar tih kapljica. Korištenjem teorije funkcionala gustoće za doprinose srednjeg polja i Lee-Huang-Yang doprinose, proširena Gross-Pitaevskii jednadžba riješena je u rotirajućem referentnom sustavu koristeći propagaciju u imaginarnom vremenu. Ključna opažanja pokazuju da je kutna količina gibanja po čestici komponente s vrtlogom dosljedno jednak $1\hbar$, što je u skladu s teorijskim predviđanjima. Osim toga, jače stiskanje rezultira samovezanijim konfiguracijama. Značajno je da je sustav više samovezan kada je vrtlog u manje brojnijoj vrsti, u usporedbi s kada je vrtlog u brojnijoj komponenti ili u obje komponente, što rezultira najmanjim vezanjem. Stiskanje duž z-osi povećava radijus kapljice u xy-ravnini, dok smanjuje njezinu debljinu u xz-ravnini, i zanimljivo, naizgled nema utjecaj na veličinu jezgre vrtloga. Dobiveni rezultati sugeriraju da bi jače stisnuti kvazi-2D sustavi mogli biti eksperimentalno izvedivi za proučavanje vrtloga.

Ključne riječi: Bose-Einsteinov kondenzat, kvantni fluid, bozonske mješavine, vrtlog

Rad sadrži: 60 stranica, 26 slika, 6 tablica, 47 literaturnih navoda. Izvornik je na engleskom jeziku.

Mentor: prof. dr. sc. Leandra Vranješ Markić

Neposredni voditelj: Prof. Dr. Jordi Boronat

Ocjenjivači: prof. dr. sc. Leandra Vranješ Markić,
izv. prof. dr. sc. Petar Stipanović,
doc. dr. sc. Martina Požar

Rad prihvaćen: 28. 08. 2024.

Rad je pohranjen u Knjižnici Prirodoslovno–matematičkog fakulteta, Sveučilišta u Splitu.

Basic documentation card

University of Split
Faculty of Science
Department of Physics
Ruđera Boškovića 33, 21000 Split, Croatia

Master thesis

Vortices in squeezed Bose-Bose quantum droplets

Ivan Poparić

University graduate study Physics, specialization in Computational Physics

Abstract:

This thesis investigates the properties of quantum droplets composed of two hyperfine states of potassium-39, confined along one axis, with a focus on the vortices within these droplets. Using Density Functional Theory for mean-field and Lee-Huang-Yang contributions, the extended Gross-Pitaevskii equation was solved in the rotating frame using imaginary time propagation. A key observation is that the angular momentum per particle of the component with a vortex consistently equals $1\hbar$, aligning with theoretical predictions. Additionally, stronger confinement (increased squeezing) results in more self-bound configurations. Notably, the system is more self-bound when the vortex is in the less numerous species, compared to when the vortex is in the more numerous component or in both components, which results in the least binding. Squeezing along the z-axis increases the droplet radius in the xy-plane while reducing its thickness in the xz-plane, and interestingly, does not appear to affect the size of the vortex core. These findings suggest that more confined quasi-2D systems could provide experimentally feasible setups for studying vortices.

Keywords: Bose-Einstein Condensate, quantum fluid, bosonic mixtures, vortex

Thesis consists of: 60 pages, 26 figures, 6 tables, 47 references. Original language: English.

Supervisor: Prof. Dr. Leandra Vranješ Markić

Leader: Prof. Dr. Jordi Boronat

Reviewers: Prof. Dr. Leandra Vranješ Markić,
Asoc. Prof. Dr. Petar Stipanović,
Assist. Prof. Dr. Martina Požar

Thesis accepted: August 28, 2024

Thesis is deposited in the library of the Faculty of Science, University of Split.

First and foremost, I would like to express my deepest gratitude to my thesis advisors, Prof. Dr. Leandra Vranješ Markić and Prof. Dr. Jordi Boronat, whose expertise and insights were instrumental in the completion of this thesis. I am also deeply thankful to my university professors, particularly Assoc. Prof. Dr. Petar Stipanović, who supervised my Bachelor's thesis and was always helpful in navigating the bureaucratic processes.

A special thanks goes to my friends and colleagues from university - Martina, Petra, Nikola, Vana, and Petra - who provided support and camaraderie throughout this journey.

I would also like to express my appreciation to my friends outside the world of physics - Josip, Robert, Luka, and Ivana - whose friendship and encouragement were invaluable during this time.

Thank you, Constantin, Eliška, and Maaike, for making my stay in Barcelona an unforgettable experience.

Finally, I am deeply grateful to my family, especially my parents, for their unwavering support. This achievement would not have been possible without them.

Contents

1 Introduction **1**

2 Basic theory of Bose gases **5**
- 2.1 Statistical Physics of The Ideal Bose Gas 5
- 2.2 Theory of the Weakly Interacting Bose Gas - Gross-Pitaevskii equation 10
- 2.3 Ground state energy of a Uniform Weakly Interacting Bose Gas 13
  - 2.3.1 Lowest-order approximation: Mean-Field 14
  - 2.3.2 Higher-order approximation 15
  - 2.3.3 Bogoliubov transformation 16
  - 2.3.4 Lee-Huang-Yang energy 18

3 Basic theory of Bose-Bose mixtures and Quantum Droplets **20**
- 3.1 Mean-field theory of Bose-Bose mixtures 20
- 3.2 Lee-Huang-Yang energy and Gross-Pitaevskii equation 22
- 3.3 Quantum droplets 23

4 Theory of Superfluids and their Rotation **25**
- 4.1 Basic theory of Superfluidity: Landau's criterion 25
- 4.2 Hydrodynamics of superfluids 26
- 4.3 Rotation of Superfluids 27
- 4.4 Bose-Einstein condensate as a superfluid 29

5 Numerical method for solving the equations **30**
- 5.1 Theoretical derivation 30
- 5.2 Algorithmic implementation 33
- 5.3 Angular momentum calculation 34

6 Non-rotating self-bound droplets **35**

7 Vortices in rotating self-bound droplets **41**
- 7.1 Angular Momentum 41
- 7.2 Droplets with vortices 41
- 7.3 Critical atom number for vortex hosting 50
- 7.4 Larger quantization vortex 51

8 Conclusion **54**

9 Bibliography **56**

1 Introduction

In classical physics, one can easily keep track of different particles and follow their individual trajectories. However, in quantum physics, no such notion exists. Quantum particles are indistinguishable, and in three-dimensional space, they fall into two categories based on their behavior when exchanged. The wave function of fermions is antisymmetric, which leads to the Pauli exclusion principle, making fermions the building blocks of our world. Bosons, on the other hand, have symmetric wave functions and, at the fundamental level, mediate forces. Composite particles, like atoms, can also exhibit quantum behavior and consequently also fall into these two categories. The distinction between the two types lies in their spin.

The spin of a quantum particle has nothing to do with classical spinning; rather, it represents an intrinsic angular momentum of the particle. The spin wave function of a quantum particle is an element of a representation space of the group $SU(2)$. Representations of the $SU(2)$ group come in symmetric and antisymmetric varieties, corresponding to bosons and fermions, respectively. At a more detailed level, integer spin representations correspond to bosons ($j = 0, 1, 2, \dots$), while odd half-integer spin representations correspond to fermions ($j = \frac{1}{2}, \frac{3}{2}, \frac{5}{2}, \dots$). Elementary particles that build our world are all spin-$\frac{1}{2}$, and since neutral atoms have the same number of protons and electrons, the number of neutrons decides whether an atom is a fermion or a boson.

Bosons exhibit a peculiar behavior at low temperatures, namely Bose-Einstein condensation (BEC). Bose-Einstein condensation originated in Albert Einstein's study of non-interacting atoms in 1925 [1], where he predicted a phase transition during which all atoms condense into the lowest energy state. His work was based on Satyendra N. Bose's study of photons [2] published in 1924.

Experimentally, two phenomena are of significance: superconductivity and superfluidity. Superconductivity was first observed in 1911 by Heike K. Onnes in mercury [3], while superfluidity in helium was discovered independently by Pyotr Kapitza [4], and John F. Allen and Don Misener [5] in 1938. That same year, Fritz London realized that Bose-Einstein condensation and superfluidity in helium-4 are connected. The λ-transition in the heat capacity of helium-4 shows a clear similarity to a spike predicted by Bose-Einstein statistics [6].

Superconductivity and superfluidity were phenomenologically described by László Tisza in 1938 using a two-fluid model [7], which treats the system as a mixture of a normal fluid and a superfluid. In 1941 Lev Landau developed the first full theory of superfluids based on elementary excitation spectrum [8], while a microscopic description of interacting Bose gases was published by Nikolay Bogoliubov in 1947 [9].

In 1951, Lev Landau and Evgeny Lifshitz [10], and Oliver Penrose [11] made significant advances in understanding the microscopic nature of superfluids by introducing the concept of

off-diagonal long-range order, which provided a quantum mechanical criterion for distinguishing between normal and superfluid phases in terms of the density matrix. This concept was instrumental in the later development of the theory. Later, in 1956, Penrose, together with Lars Onsager, expanded upon this work, generalizing the mathematical description of BEC to include systems of interacting particles [12].

In 1949, Onsager had already laid the groundwork for the understanding of rotating BECs by introducing the concept of quantized vortices in superfluids [13]. This quantization is a hallmark of superfluid behavior. Richard Feynman contributed to the understanding of superfluidity in 1955 by developing a path-integral formulation of quantum mechanics that could be applied to superfluids. He used this approach to describe the properties of superfluid helium-4 [14]. Feynman's work provided a powerful tool for studying superfluid systems and contributed to the broader understanding of quantum fluids.

In 1956, H. E. Hall and W. F. Vinen experimentally confirmed the existence of quantized vortices in superfluid helium-4. Their experiments provided the first direct evidence of these quantized structures, validating the theoretical predictions made by Onsager and Feynman [15]. This discovery was a pivotal moment in the study of superfluids, as it confirmed the quantum mechanical nature of superfluidity at a macroscopic scale.

Finally, in 1957, T. D. Lee, K. Huang, and C. N. Yang made a groundbreaking contribution by developing a microscopic theory of Bose-Einstein condensation in interacting Bose gases. Their work extended Bogoliubov's earlier theory by considering the higher order effects of interactions between particles in a Bose gas, leading to a more accurate description of the properties of superfluid helium-4 [16]. This theoretical advancement provided deeper insights into the nature of Bose-Einstein condensates.

The invention of the laser by Theodore Maiman in 1960 [17] and the subsequent development of lasers in the 1960s revolutionized the experimental study of quantum systems, providing a powerful tool for the precise manipulation and control of atomic and molecular systems. This advancement enabled a wide range of experiments, making lasers essential for cooling and trapping atoms and paving the way for the development of techniques such as laser cooling and magneto-optical traps (MOTs).

In the late 1970s and 1980s, laser cooling techniques enabled the creation of ultra-cold atomic systems, where quantum phenomena could be observed on a macroscopic scale. Critical to this development were magneto-optical traps (MOTs), developed in the late 1980s. MOTs use a combination of laser cooling and magnetic fields to trap neutral atoms in a small region of space, where they can be cooled to microkelvin temperatures [18].

These developments culminated in 1995, when Eric Cornell and Carl Wieman at the University of Colorado, Boulder, and Wolfgang Ketterle at the Massachusetts Institute of Technology (MIT), independently achieved Bose-Einstein condensation in dilute gases of

alkali atoms [19, 20]. Cornell and Wieman's group created a BEC using rubidium-87 atoms, while Ketterle's group achieved BEC with sodium atoms.

The experimental discovery of a Bose-Einstein Condensate in 1995 was a landmark achievement in condensed matter physics, as it provided the first direct observation of the state of matter predicted by Einstein and Bose in the 1920s. This breakthrough opened new avenues of research, leading to advancements in areas such as quantum computing, precision measurements, and the study of quantum many-body systems. For their work, Cornell, Wieman, and Ketterle were awarded the Nobel Prize in Physics in 2001. Their discovery continues to be influential, with BECs remaining a key part of modern atomic, molecular, and optical physics [21].

Quantum droplets, self-bound states of ultracold atoms, emerge from the interplay of attractive and repulsive forces within ultracold quantum gases. These droplets exhibit fascinating behaviors, distinct from classical liquid droplets, driven by quantum fluctuations and many-body interactions. Quantum droplets arise due to the delicate balance between mean-field attractions and repulsive forces that are stabilized by quantum fluctuations [22]. The density of quantum droplets is significantly lower than that of conventional liquids, such as helium or even air, making them a unique state of matter. Experimentally observed potassium droplets have a density on the order of $\sim 10^{-9} - 10^{-8}$ g/cm^3 [23, 24], which is several orders of magnitude lower than that of liquid helium (0.145 g/cm^3) [25] and even air ($1.2 \cdot 10^{-3}$ g/cm^3) [26].

In ultracold atomic systems, the interaction between atoms can be finely tuned using external magnetic fields through a technique known as Feshbach resonance [27]. This allows for precise control over the strength and nature (attractive or repulsive) of the interatomic forces, making it possible to explore a wide variety of quantum states, including quantum droplets. For instance, in a BEC of dysprosium or erbium atoms, where dipole-dipole interactions play a significant role, the competition between long-range dipolar attractions and short-range contact repulsions can give rise to self-bound states [28].

One of the most interesting aspects of quantum droplets is their ability to remain stable even without external confinement [29]. This self-bound nature results in quantum droplets that are essentially isolated from their environment, making them ideal for studying fundamental quantum effects in a controlled manner. Moreover, these droplets can exhibit a form of quantum coherence similar to that seen in superfluids [30].

Furthermore, quantum droplets enable the exploration of the interplay between quantum mechanics and fluid dynamics, giving rise to phenomena such as pattern formation in so-called supersolids [31]. These phenomena are not only of fundamental interest but also hold potential applications in developing new quantum technologies, including precision measurement devices, quantum simulators, and quantum computers.

As research in this field advances, the ongoing exploration of quantum droplets in ultracold atomic systems promises to deepen our understanding of quantum many-body physics. The versatility and tunability of atomic systems ensure that they will remain at the forefront of this area of research, with the potential to uncover novel quantum phenomena. Quantum droplets have been observed in homonuclear mixtures of two hyperfine states of ^{39}K [23, 24], as well as in heteronuclear mixtures of ^{41}K-^{87}Rb [32] and ^{23}Na-^{87}Rb [33]. One difficulty in experimental realization is the number of atoms required. However, this can be reduced by squeezing the droplet in one direction [34].

Vortices are yet to be observed in Bose-Bose quantum droplets. They have been theoretically investigated in 3D droplets of heteronuclear mixtures of ^{41}K-^{87}Rb [35], where the critical atom number for hosting vortices was determined. This analysis has not yet been performed for homonuclear mixtures of ^{39}K, and predictions for the critical atom number under experimentally attainable parameters for squeezed droplets are of particular interest. The aim of this thesis is to study vortices in squeezed homonuclear mixtures of ^{39}K, determine the optimal configuration for a vortex in such mixtures, and find the critical number of atoms for vortex hosting.

The structure of this thesis is organized as follows: Chapter 2 introduces the fundamental theory of Bose gases, covering topics such as the ideal gas, the Gross-Pitaevskii equation, weakly interacting gases, and the Bogoliubov transformation. In Chapter 3, the focus shifts to bosonic mixtures and the concept of quantum droplets. Chapter 4 delves into the study of superfluids, particularly discussing their rotational properties. The methodology employed throughout the thesis is detailed in Chapter 5. Simulation results are presented in two parts: Chapter 6 covers the findings for non-rotating quantum droplets, while Chapter 7 addresses the behavior of rotating quantum droplets with vortices. Finally, Chapter 8 offers concluding remarks and a summary of the thesis.

2 Basic theory of Bose gases

In this section, we delve into the fundamental theory necessary for a comprehensive understanding of this thesis. The approach is primarily based on the work of Lev Pitaevskii and Sandro Stringari, as detailed in their book [36], with parts taken from Christopher Pethick's and Henrik Smith's book [37].

2.1 Statistical Physics of The Ideal Bose Gas

Statistical description of a Bose gas is the simplest in the grand canonical ensemble. What follows is a description of the grand canonical ensemble and it's application in quantum many body theory.

The grand canonical ensemble describes a system in thermodynamic equilibrium that exchanges energy and particles with a reservoir. It is typically parameterized by the reservoir's chemical potential μ, temperature T, and the system's volume V.

Quantum systems are described by their Hamiltonians, eigenstates, and eigenvalues, which correspond to possible energies. The configuration of N_k particles in an eigenstate k with energy E_k has a probability of realization given by

$$P_{N_k}(E_k) = e^{\beta(\mu N_k - E_k)}, \tag{2.1}$$

where $\beta = \frac{1}{k_B T}$. Thus, the grand canonical partition function is

$$Z(\beta, \mu) = \sum_{N_k=0}^{\infty} \sum_k P_{N_k}(E_k) = \sum_{N_k=0}^{\infty} \sum_k e^{\beta(\mu N_k - E_k)}. \tag{2.2}$$

Here, one can notice the canonical partition function

$$Q_{N_k}(\beta) = \sum_k e^{-\beta E_k}, \tag{2.3}$$

so the grand canonical partition function can be written as

$$Z(\beta, \mu) = \sum_{N_k=0}^{\infty} e^{\beta(\mu N_k)} Q_{N_k}(\beta). \tag{2.4}$$

Once the partition function is known, other thermodynamic properties of the system can be calculated from the grand canonical potential

$$\Omega = -k_B T \ln Z, \tag{2.5}$$

since it is defined as

$$\Omega = E - TS - \mu N. \tag{2.6}$$

This gives the entropy of the system

$$S = -\frac{\partial \Omega}{\partial T}, \tag{2.7}$$

the total number of particles

$$N \equiv \langle N \rangle = -\frac{\partial \Omega}{\partial \mu}, \tag{2.8}$$

and energy

$$E \equiv \langle E \rangle = \Omega - T\frac{\partial \Omega}{\partial T} - \mu \frac{\partial \Omega}{\partial \mu}. \tag{2.9}$$

A non-interacting quantum system is described by an independent Hamiltonian

$$\hat{H} = \sum_j \hat{H}_j^{(1)}, \tag{2.10}$$

where $\hat{H}_j^{(1)}$ is the single-particle Hamiltonian and the sum over j includes all particles. The solution boils down to solving a single-particle Schrödinger equation

$$\hat{H}_j^{(1)} \phi_i(\vec{r}) = \epsilon_i \phi_i(\vec{r}), \tag{2.11}$$

where the eigenstate of the full Hamiltonian, k, is given by the set of occupation numbers n_i of single-particle states and corresponding energies ϵ_i, such that $N_k = \sum_i n_i$ and $E_k = \sum_i \epsilon_i n_i$.

With this in mind, the grand canonical partition function can be written as

$$\begin{aligned} Z(\beta, \mu) &= \sum_{N_k=0}^{\infty} \sum_k e^{\beta(\mu N_k - E_k)} \\ &= \prod_i \sum_{n_i=0}^{\infty} \left[e^{\beta(\mu - \epsilon_i)} \right]^{n_i} \\ &= \left\{ \sum_{n_0=0}^{\infty} \left[e^{\beta(\mu-\epsilon_0)} \right]^{n_0} \right\} \cdot \left\{ \sum_{n_1=0}^{\infty} \left[e^{\beta(\mu-\epsilon_1)} \right]^{n_1} \right\} \cdot \ldots . \end{aligned} \tag{2.12}$$

Here, one can recognize the geometric series $\sum_{k=0}^{\infty} ax^k = a(1-x)^{-1}$ for $|x| < 1$. Plugging this into the equation (2.5) for the grand potential Ω yields

$$\Omega = -k_{\mathrm{B}} T \ln Z = k_{\mathrm{B}} T \sum_i \ln \left(1 - e^{\beta(\mu - \epsilon_i)} \right), \tag{2.13}$$

from which it follows, using (2.8), that the total number of particles is

$$N = \sum_i \left[e^{\beta(\epsilon_i - \mu)} - 1 \right]^{-1} = \sum_i \langle n_i \rangle . \tag{2.14}$$

The average occupation number of single-particle states $\langle n_i \rangle$ is thus defined by the Bose-Einstein distribution function

$$\langle n_i \rangle = \frac{1}{e^{\beta(\epsilon_i - \mu)} - 1}. \tag{2.15}$$

Consequently, it follows that the energy of the system is given by

$$E = \sum_i \frac{\epsilon_i}{e^{\beta(\epsilon_i - \mu)} - 1}. \tag{2.16}$$

A consequence of equation (2.15) is that, since the occupation number must always be greater than or equal to zero, the chemical potential must be lower than the lowest eigenenergy of the single-particle Hamiltonian, $\mu < \epsilon_0$.

Bose-Einstein condensation emerges from the fact that the occupation number of the lowest energy state $N_0 \equiv \langle n_0 \rangle$ grows as $\mu \to \epsilon_0$. The equation (2.14) can be written as

$$N = \langle n_0 \rangle + \sum_{i \neq 0} \langle n_i \rangle \equiv N_0 + N_T, \tag{2.17}$$

where N_T is called the thermal component and corresponds to the number of particles outside of the condensate, while N_0 are particles in the condensate.

At a given temperature T, N_0 as a function of the chemical potential diverges as $\mu \to \epsilon_0$, while N_T reaches its maximum value of N_c. This behavior can be seen plotted in Figure 1. The critical value N_c changes with temperature, and at temperatures higher than T_c it holds that $N_c(T) = N_T(T, \mu = \epsilon_0) > N$. In that case, $N = N_0 + N_T$ is valid for $\mu < \epsilon_0$, and consequently $N_T \gg N_0$. Decreasing the temperature, eventually one reaches a critical temperature T_c, such that

$$N_c(T_c) = N_T(T_c, \mu = \epsilon_0) = N, \tag{2.18}$$

and at temperatures below that, the thermal component alone cannot satisfy the condition $N = N_0 + N_T$, so the condensed component becomes meaningfully large. Temperature T_c is the critical temperature at which Bose-Einstein condensation takes place.

Better insight may be attained by applying this formalism to a gas in a box of volume V. Since the gas is ideal, the single-particle Hamiltonian is given by

$$\hat{H}^{(1)} = \frac{p^2}{2m}. \tag{2.19}$$

With standard periodic boundary conditions, the solutions to the Schrödinger equation are plane waves

$$\phi_{\vec{p}} = \frac{1}{\sqrt{V}} e^{\frac{i}{\hbar}\vec{p}\cdot\vec{r}}, \tag{2.20}$$

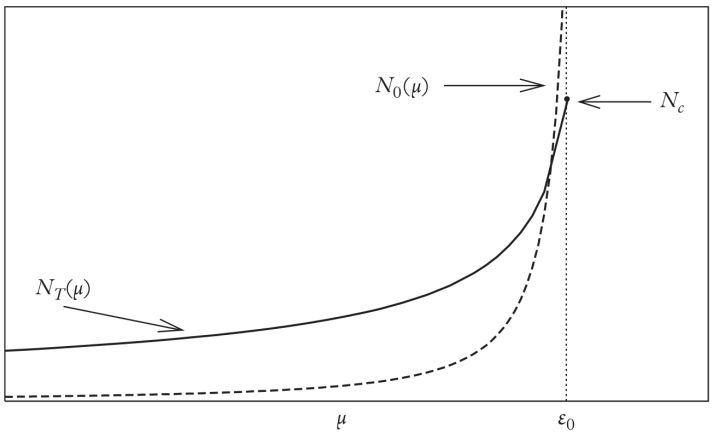

Figure 1: *The number of particles in the condensed (N_0, dashed) and thermal (N_T, solid) components plotted as functions of the chemical potential μ at a fixed temperature T. Taken from [36].*

whose energies are

$$\epsilon_{\vec{p}} = \frac{p^2}{2m}. \tag{2.21}$$

Momentum is given by

$$\vec{p} = \frac{2\pi\hbar}{L}\vec{n}, \tag{2.22}$$

where $L = V^{1/3}$ and $\vec{n} = (n_x, n_y, n_z)$.

The lowest energy state is $p = 0$, with $\epsilon_0 = 0$, thus the chemical potential has to be negative. The number of atoms in the excited states can be calculated as

$$N_T = \sum_{p\neq 0} \frac{1}{e^{\beta(\epsilon_p - \mu)} - 1} = \sum_{p\neq 0} \frac{1}{e^{\beta(p^2/2m - \mu)} - 1}, \tag{2.23}$$

which can be easily done by integrating over $\vec{p}$-space instead of summing over states. Concretely, when the thermal energy is much greater than the energy difference between eigenenergies, $k_{\mathrm{B}}T \gg \frac{h^2}{2mV^{2/3}}$, one can do a substitution

$$\sum_{\vec{p}} \to \frac{V}{2\pi h^3} \int \mathrm{d}\vec{p}, \tag{2.24}$$

so

$$N_T = \frac{V}{2\pi h^3} \int \mathrm{d}\vec{p} \frac{1}{e^{\beta(p^2/2m - \mu)} - 1}. \tag{2.25}$$

This works out to be

$$N_T = \frac{V}{\lambda_T^3} g_{3/2}(e^{\beta\mu}), \tag{2.26}$$

where λ_T is the thermal de Broglie wavelength

$$\lambda_T = \sqrt{\frac{2\pi\hbar^2}{m k_{\mathrm{B}} T}}. \tag{2.27}$$

The function $g_p(z)$ is a Bose function

$$g_p(z) = \frac{1}{\Gamma(p)} \int_0^\infty \mathrm{d}x \frac{x^{p-1}}{z^{-1}e^x - 1} = \sum_{l=1}^{\infty} \frac{z^l}{l^p}, \tag{2.28}$$

which in the case at hand works out to be

$$g_{3/2}(z) = \frac{2}{\sqrt{\pi}} \int_0^\infty \mathrm{d}x \frac{x^{1/2}}{z^{-1}e^x - 1}. \tag{2.29}$$

The quantity $z = e^{\beta\mu}$ is known as fugacity. In the case of $z = 1$, the Bose function (2.28) boils down to a Riemann zeta function:

$$\zeta(s) = \sum_{n=1}^{\infty} \frac{1}{n^s}, \tag{2.30}$$

where $s \in \mathbb{C}$, and $\mathrm{Re}(s) > 1$ [38].

From the condition (2.18), the result for the critical temperature for Bose-Einstein condensation follows:

$$k_\mathrm{B} T_\mathrm{c} = \frac{2\pi\hbar^2}{m g_{3/2}(1)^{2/3}} \left(\frac{N}{V}\right)^{2/3}. \tag{2.31}$$

Since at higher temperatures $N_T \gg N_0$, the chemical potential can be obtained from $N_T = N$; while at temperatures below T_c one sets $\mu = 0$ in N_T [36, p. 20, 3.30].

Substituting the thermal wavelength λ_T into (2.26), with $\mu = 0$, yields

$$N_T = \left(\frac{m k_\mathrm{B} T}{2\pi\hbar^2}\right)^{3/2} V g_{3/2}(1), \tag{2.32}$$

which together with the critical temperature T_c, as defined in (2.31), simplifies to

$$N_T = \left(\frac{T}{T_c}\right)^{3/2} N. \tag{2.33}$$

The number of particles in the condensate is simply

$$N_0(T) = \left[1 - \left(\frac{T}{T_c}\right)^{3/2}\right] N. \tag{2.34}$$

The ratio of the number of condensed particles to the total number of particles, N_0/N, is called the condensate fraction. Observing the equation (2.34) leads to the conclusion that at absolute zero, $T = 0$, all particles of the ideal Bose gas will be condensed, while at temperatures higher than T_c, no particles will be in the condensate. The condensate fraction as a function of temperature is shown in Figure 2.

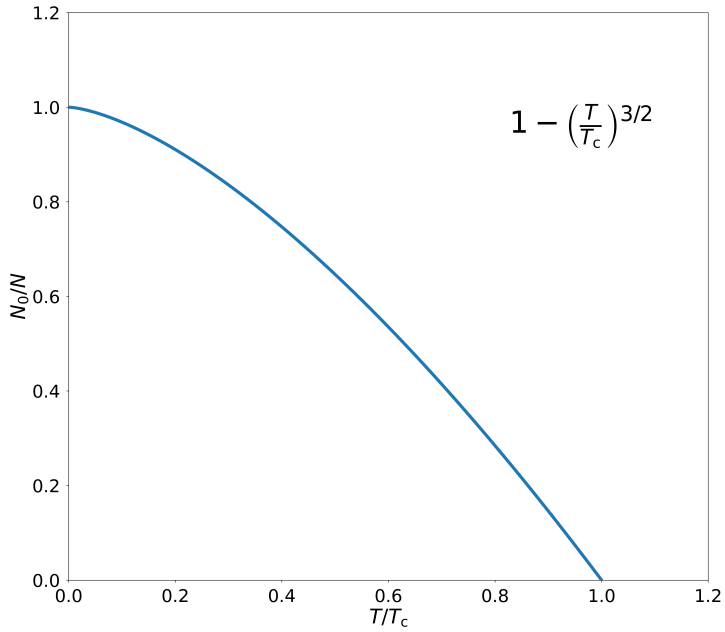

Figure 2: *Condensate fraction as a function of temperature for an ideal Bose gas in a box.*

2.2 Theory of the Weakly Interacting Bose Gas - Gross-Pitaevskii equation

The ideal Bose gas lacks particle interactions, which cannot be completely ignored even in very dilute gases. Traditional perturbation techniques fail, which is why Bogoliubov theory [9] is used, which introduces an order parameter whose evolution follows the Gross-Pitaevskii equation [39, 40].

Dilute gases are characterized by the condition

$$r_0 \ll d, \tag{2.35}$$

where the range of interatomic forces, r_0, is much smaller than the average distance between the atoms, d. The distance d is determined by the gas density as $d = (N/V)^{-1/3} = n^{-1/3}$. Consequently, out of all possible many-body interactions, only two-body interactions need to be taken into account.

The large distances between atoms in a dilute gas allow for the use of the asymptotic form of the wave function for the relative motion of two atoms, determined by the scattering amplitude. When the condition

$$\frac{pr_0}{\hbar} \ll 1 \tag{2.36}$$

is satisfied for all non-negligible momenta, the scattering amplitude becomes independent of both energy and scattering angle. In this regime, the scattering amplitude can be approximated by its lowest energy value, which is determined by the s-wave scattering length a.

This single parameter, the s-wave scattering length a, effectively encapsulates all the interactions' effects on the physical properties of the gas. The gas is considered weakly interacting if the gas parameter is small

$$n|a|^3 \ll 1, \tag{2.37}$$

which is equivalent to the condition that the scattering length is much smaller than the interatomic distances

$$|a| \ll d. \tag{2.38}$$

For a proper description of bosons in a dilute gas, the starting point should be their most general Hamiltonian expressed using the language of quantum field theory

$$\begin{aligned}\hat{\mathscr{H}} = &\int \mathrm{d}\vec{r}\left(\frac{\hbar^2}{2m}\nabla\hat{\Psi}^\dagger(\vec{r})\nabla\hat{\Psi}(\vec{r})\right) + \int \mathrm{d}\vec{r}\hat{\Psi}^\dagger(\vec{r})V_{\text{ext}}(\vec{r})\hat{\Psi}(\vec{r}) \\ &+ \frac{1}{2}\int \mathrm{d}\vec{r'}\mathrm{d}\vec{r}\hat{\Psi}^\dagger(\vec{r'})\hat{\Psi}^\dagger(\vec{r})V(\vec{r'}-\vec{r})\hat{\Psi}(\vec{r'})\hat{\Psi}(\vec{r}),\end{aligned} \tag{2.39}$$

where $\hat{\Psi}(\vec{r})$ is the field operator, and $V(\vec{r'}-\vec{r})$ is the two-body potential, and $V_{\text{ext}}(\vec{r})$ the external potential. The field operators create or annihilate a particle at $\vec{r}$, and they obey the following commutation relations:

$$\left[\hat{\Psi}(\vec{r}), \hat{\Psi}^\dagger(\vec{r'})\right] = \delta(\vec{r}-\vec{r'}), \tag{2.40}$$

and

$$\left[\hat{\Psi}(\vec{r}), \hat{\Psi}(\vec{r'})\right] = \left[\hat{\Psi}^\dagger(\vec{r}), \hat{\Psi}^\dagger(\vec{r'})\right] = 0. \tag{2.41}$$

The field operator also defines the one-body density matrix

$$n^{(1)}(\vec{r}, \vec{r'}) = \left\langle \hat{\Psi}^\dagger(\vec{r})\hat{\Psi}(\vec{r'})\right\rangle, \tag{2.42}$$

which, when $\vec{r} = \vec{r'}$, becomes the diagonal density of the system $n(\vec{r})$. The total number of particles is then given by

$$N = \int \mathrm{d}\vec{r}n(\vec{r}). \tag{2.43}$$

The field operator $\hat{\Psi}(\vec{r})$ can be expressed in terms of single-particle states $\psi_i(\vec{r})$ and their annihilation (creation) operators $\hat{a}_i$ ($\hat{a}_i^\dagger$) as

$$\hat{\Psi}(\vec{r}) = \sum_i \psi_i(\vec{r})\hat{a}_i, \tag{2.44}$$

where the operators obey the commutation relations analogous to (2.40) and (2.41):

$$\left[\hat{a}_i, \hat{a}_j^\dagger\right] = \delta_{ij}, \tag{2.45}$$

and

$$[\hat{a}_i, \hat{a}_j] = \left[\hat{a}_i^\dagger, \hat{a}_j^\dagger\right] = 0. \tag{2.46}$$

Single-particle wave functions $\psi_i(\vec{r})$ form a complete orthonormal set. The expectation value

$$\langle \hat{a}_i^\dagger \hat{a}_i \rangle = N_i \tag{2.47}$$

gives the occupation number of the i-th single-particle state.

To arrive at an equation for the time evolution of the field, the Heisenberg picture of quantum mechanics will be employed. In the Heisenberg picture, the equation of motion for the field operator is

$$i\hbar \frac{\partial}{\partial t} \hat{\Psi}(\vec{r}, t) = \left[\hat{\Psi}(\vec{r}, t), \hat{\mathscr{H}}\right], \tag{2.48}$$

which, when taking the Hamiltonian to be (2.39), becomes

$$i\hbar \frac{\partial}{\partial t} \hat{\Psi}(\vec{r}, t) = \left[-\frac{\hbar^2}{2m}\nabla^2 + V_{\text{ext}}(\vec{r}) + \int \mathrm{d}\vec{r'}\, \hat{\Psi}^\dagger(\vec{r'}, t) V(\vec{r'} - \vec{r}) \hat{\Psi}(\vec{r'}, t)\right] \hat{\Psi}(\vec{r}, t). \tag{2.49}$$

From this point, Bogoliubov theory enables an effective description of the condensate's properties without assumptions about the energy spectrum [9]. Bogoliubov theory boils down to the following [9]:

a) The microscopic interaction potential $V(\vec{r'} - \vec{r})$ is replaced by an effective potential V_{eff}, to which perturbation theory and Born approximation can be applied.

b) The number of condensed particles is much larger than unity, $N_0 = \langle \hat{a}_0^\dagger \hat{a}_0 \rangle \gg 1$, so the commutation relation

$$\left[\hat{a}_0, \hat{a}_0^\dagger\right] = \delta_{00} = 1, \tag{2.50}$$

is much smaller than $\hat{a}_0$ and $\hat{a}_0^\dagger$. Thus, operators $\hat{a}_0$ and $\hat{a}_0^\dagger$ can be treated as numbers, $\hat{a}_0 = \sqrt{N_0}$, and their non-commutativity ignored.

c) The field operator (2.44) is expressed as

$$\begin{aligned} \hat{\Psi}(\vec{r}) &= \psi_0(\vec{r})\hat{a}_0 + \sum_{i>0} \psi_i(\vec{r})\hat{a}_i \\ &= \psi_0(\vec{r})\sqrt{N_0} + \sum_{i>0} \psi_i(\vec{r})\hat{a}_i \\ &= \Psi_0(\vec{r}) + \delta\hat{\Psi}(\vec{r}), \end{aligned} \tag{2.51}$$

where $\Psi_0(\vec{r}) = \psi_0(\vec{r})\sqrt{N_0}$ represents the macroscopic, condensed component of the field.

Bogoliubov theory works for macroscopic phenomena of Bose-Einstein condensates. One can think of it as replacing the macroscopic, condensed component of the field operator with a classical field $\Psi_0(\vec{r})$, called the order parameter. The order parameter is also known as the wave

function of the condensate. Above the critical temperature for Bose-Einstein condensation, the order parameter vanishes. Bogoliubov theory is in a way equivalent to the transition from quantum electrodynamics to classical Maxwell's theory. The order parameter can be expressed as

$$\Psi_0(\vec{r}) = |\Psi_0(\vec{r})| \exp\left(iS(\vec{r})\right), \tag{2.52}$$

where the modulus squared $|\Psi_0(\vec{r})|^2 = \rho(\vec{r})$ represents the condensate density, while $S(\vec{r})$ is the phase.

Working within this framework, and assuming that the order parameter varies slowly over distances comparable to the range of interactions, the equation (2.49) simplifies to the Gross-Pitaevskii equation (GPE)

$$i\hbar\frac{\partial}{\partial t}\Psi(\vec{r},t) = \left[-\frac{\hbar^2}{2m}\nabla^2 + V_{\text{ext}}(\vec{r}) + g|\Psi(\vec{r},t)|^2\right]\Psi(\vec{r},t), \tag{2.53}$$

where the coupling constant $g = \int \mathrm{d}\vec{r} V_{\text{eff}} = \frac{4\pi\hbar^2 a}{m}$ characterizes the interaction strength, with a being the s-wave scattering length. The GPE is a nonlinear Schrödinger equation, reflecting the interaction between particles in the condensate through the term $g|\Psi(\vec{r},t)|^2$, which depends on the density of the condensate.

2.3 Ground state energy of a Uniform Weakly Interacting Bose Gas

Consider a dilute uniform Bose gas of N particles contained within a box of volume V, with the Hamiltonian (2.39) without the external potential. In that case, the field operator can be expressed in terms of momentum state operators

$$\hat{\Psi}(\vec{r}) = \sum_{\vec{p}} \frac{1}{V^{1/2}} e^{\frac{i}{\hbar}\vec{p}\cdot\vec{r}}\hat{a}_{\vec{p}}, \tag{2.54}$$

where momentum $\vec{p}$ satisfies periodic boundary conditions and $\hat{a}_{\vec{p}}$ annihilates a particle in the state with momentum $\vec{p}$. Using this operator, the Hamiltonian (2.39) becomes

$$\hat{\mathscr{H}} = \sum_{\vec{p}} \frac{p^2}{2m}\hat{a}^\dagger_{\vec{p}}\hat{a}_{\vec{p}} + \frac{1}{2V}\sum_{\vec{p_1},\vec{p_2},\vec{q}} V_{\vec{q}}\hat{a}^\dagger_{\vec{p_1}+\vec{q}}\hat{a}^\dagger_{\vec{p_2}-\vec{q}}\hat{a}_{\vec{p_1}}\hat{a}_{\vec{p_2}}, \tag{2.55}$$

where $V_{\vec{q}}$ is given by

$$V_{\vec{q}} = \int \mathrm{d}\vec{r} V(\vec{r}) e^{-\frac{i}{\hbar}\vec{q}\cdot\vec{r}}. \tag{2.56}$$

2.3.1 Lowest-order approximation: Mean-Field

Following the requirements for the application of Bogoliubov theory, the microscopic interaction potential $V(\vec{r})$ is replaced by an effective potential $V_{\text{eff}}(r)$. Since in dilute gases only small momenta meaningfully contribute — effectively contact interactions — consideration can be restricted to the $q = 0$ value of the Fourier transform (2.56), and $V_{\vec{q}}$ in the Hamiltonian (2.55) can be replaced by V_0 given by

$$V_0 = \int \mathrm{d}\vec{r}\, V_{\text{eff}}(r) = g, \tag{2.57}$$

which corresponds to the interaction strength g. This permits the phrasing of the Hamiltonian (2.55) as

$$\hat{\mathscr{H}} = \sum_{\vec{p}} \frac{p^2}{2m} \hat{a}^\dagger_{\vec{p}} \hat{a}_{\vec{p}} + \frac{V_0}{2V} \sum_{\vec{p_1},\vec{p_2},\vec{q}} \hat{a}^\dagger_{\vec{p_1}+\vec{q}} \hat{a}^\dagger_{\vec{p_2}-\vec{q}} \hat{a}_{\vec{p_1}} \hat{a}_{\vec{p_2}}, \tag{2.58}$$

to which Bogoliubov theory is applied, replacing $\hat{a}_0 = \sqrt{N_0}$.

The ground state is a zero-momentum state, $\vec{p} = 0$, and in the first approximation, it contains all atoms, i.e. $N_0 = N$. Then the ground state energy follows from (2.58) as

$$E_0 = \frac{V_0 N^2}{2V} = \frac{1}{2} N g \rho, \tag{2.59}$$

where $\rho = N/V$ is the gas density. This result is the mean-field (MF) solution.

From the ground state energy (2.59), it follows that the chemical potential is

$$\mu = \frac{\partial E_0}{\partial N} = g\rho, \tag{2.60}$$

which is positive even at absolute zero.

The pressure of a Bose gas is found to be

$$P = -\frac{\partial E_0}{\partial V} = \frac{1}{2} g \rho^2, \tag{2.61}$$

while the compressibility is given by

$$\frac{\partial \rho}{\partial P} = \frac{1}{g\rho}. \tag{2.62}$$

The sound velocity c can be found using the hydrodynamic relation

$$\frac{1}{mc^2} = \frac{\partial \rho}{\partial P}, \tag{2.63}$$

and it works out to be

$$c = \sqrt{\frac{g\rho}{m}}. \tag{2.64}$$

Using the sound velocity, the chemical potential of a dilute gas (2.60) can be written as

$$\mu = mc^2. \tag{2.65}$$

2.3.2 Higher-order approximation

To attain higher-order corrections, additional terms must be considered in the Hamiltonian (2.58), as the approximation $N_0 = N$ is not generally true. In the interaction term of the Hamiltonian, there are four momenta involved, and they can be classified as follows [16]:

a) All momenta equal to 0, with $\vec{q} = 0$. Using only these contributions gives rise to the aforementioned mean-field result. This scenario takes into account only the condensed atoms.

b) Two of the momenta equal to 0, i.e., quadratic in $\hat{a}_{\vec{p}}$ for $\vec{p} \neq 0$. This includes scattering between atoms in the single-particle ground state and excited states, which are leading-order corrections beyond the mean-field theory.

c) One of the momenta equal to 0. This contribution is generally negligible.

d) None of the momenta equal to 0. This contribution is also generally negligible.

The first correction to the result (2.59) can be derived by considering the terms quadratic in $\hat{a}_{\vec{p}}$ for $\vec{p} \neq 0$ in the Hamiltonian (2.58). This effectively means considering terms where $|\vec{q}| = |\vec{p_1}| = |\vec{p_2}|$. Then the Hamiltonian (2.58) can be expressed as

$$\hat{\mathscr{H}} = \sum_{\vec{p}} \frac{p^2}{2m} \hat{a}^\dagger_{\vec{p}} \hat{a}_{\vec{p}} + \frac{V_0}{2V} \hat{a}^\dagger_0 \hat{a}^\dagger_0 \hat{a}_0 \hat{a}_0 + \frac{V_0}{2V} \sum_{\vec{p} \neq 0} \left(4 \hat{a}^\dagger_0 \hat{a}^\dagger_{\vec{p}} \hat{a}_0 \hat{a}_{\vec{p}} + \hat{a}^\dagger_{\vec{p}} \hat{a}^\dagger_{-\vec{p}} \hat{a}_0 \hat{a}_0 + \hat{a}^\dagger_0 \hat{a}^\dagger_0 \hat{a}_{\vec{p}} \hat{a}_{-\vec{p}} \right), \tag{2.66}$$

with

$$V_0 = \int \mathrm{d}\vec{r} V_{\text{eff}}(r), \tag{2.67}$$

being the $q = 0$ value of the Fourier transform (2.56) of the effective potential. The normalization is given by the condition

$$\hat{a}^\dagger_0 \hat{a}_0 + \sum_{\vec{p} \neq 0} \hat{a}^\dagger_{\vec{p}} \hat{a}_{\vec{p}} = N, \tag{2.68}$$

since it is no longer possible to generally approximate $N_0 = N$. Using the above condition, and neglecting higher order terms results in

$$N_0^2 \approx N^2 - 2N \sum_{\vec{p} \neq 0} \hat{a}^\dagger_{\vec{p}} \hat{a}_{\vec{p}}, \tag{2.69}$$

so that when applying Bogoliubov theory in the ground state term $\hat{a}_0 = \sqrt{N_0}$ is used. The second sum in the Hamiltonian (2.66) contains the following contributions:

- Scattering of one atom from the condensate and one non-condensed atom, which can occur in four distinct ways.
- Scattering of two atoms with momenta $+\vec{p}$ and $-\vec{p}$ into the ground state.
- Scattering of two atoms from the ground state, exiting with momenta $+\vec{p}$ and $-\vec{p}$.

In this sum $\hat{a}_0 = \sqrt{N}$ is a valid approximation.

The lowest-order Born approximation for the two-body interaction is not sufficient in this case, so higher-order perturbation theory is required. It yields

$$V_0 = g\left(1 + \frac{g}{V}\sum_{\vec{p}\neq 0}\frac{m}{p^2}\right), \tag{2.70}$$

where g is the coupling constant given by $g = \frac{4\pi\hbar^2 a}{m}$. The second term in (2.70) diverges as $p \to \infty$, since the constant V_0 poorly approximates the real $V_{\vec{q}}$ matrix element at larger momenta.

Using the expressions (2.69) and (2.70), the Hamiltonian (2.66) can be written as

$$\hat{\mathscr{H}} = \sum_{\vec{p}}\frac{p^2}{2m}\hat{a}^\dagger_{\vec{p}}\hat{a}_{\vec{p}} + \frac{gN^2}{2V} + \frac{gN}{2V}\sum_{\vec{p}\neq 0}\left(2\hat{a}^\dagger_{\vec{p}}\hat{a}_{\vec{p}} + \hat{a}^\dagger_{\vec{p}}\hat{a}^\dagger_{-\vec{p}} + \hat{a}_{\vec{p}}\hat{a}_{-\vec{p}} + gm\frac{N}{V}\frac{1}{p^2}\right). \tag{2.71}$$

This Hamiltonian can be expressed in a symmetrical form

$$\hat{\mathscr{H}} = \frac{1}{2}gN\rho\left(1 + \frac{g}{V}\sum_{\vec{p}\neq 0}\frac{m}{p^2}\right) + {\sum_{\vec{p}\neq 0}}'\left[\left(\frac{p^2}{2m} + g\rho\right)\left(\hat{a}^\dagger_{\vec{p}}\hat{a}_{\vec{p}} + \hat{a}^\dagger_{-\vec{p}}\hat{a}_{-\vec{p}}\right) + g\rho\left(\hat{a}^\dagger_{\vec{p}}\hat{a}^\dagger_{-\vec{p}} + \hat{a}_{\vec{p}}\hat{a}_{-\vec{p}}\right)\right], \tag{2.72}$$

where the prime denotes a sum over one half of momentum space and $\rho = N/V$ is gas density. This Hamiltonian is diagonalizable by a Bogoliubov transformation [37].

2.3.3 Bogoliubov transformation

The Hamiltonian of the form

$$\hat{h} = \epsilon_0\left(\hat{a}^\dagger\hat{a} + \hat{b}^\dagger\hat{b}\right) + \epsilon_1\left(\hat{a}^\dagger\hat{b}^\dagger + \hat{b}\hat{a}\right), \tag{2.73}$$

where ϵ_i are constants, can be diagonalized using a Bogoliubov transformation:

$$\hat{\alpha} = u\hat{a} + v\hat{b}^\dagger, \tag{2.74}$$

$$\hat{\beta} = u\hat{b} + v\hat{a}^\dagger, \tag{2.75}$$

where u and v are transformation coefficients, which are taken to be real for simplicity. The inverse transformation is given by:

$$\hat{a} = u\hat{\alpha} - v\hat{\beta}^\dagger, \tag{2.76}$$

$$\hat{b} = u\hat{\beta} - v\hat{\alpha}^\dagger. \tag{2.77}$$

The new operators $\hat{\alpha}$ and $\hat{\beta}$ satisfy the commutation relations:

$$\left[\hat{\alpha}, \hat{\alpha}^\dagger\right] = \left[\hat{\beta}, \hat{\beta}^\dagger\right] = 1, \tag{2.78}$$

and

$$\left[\hat{\alpha}, \hat{\beta}^\dagger\right] = \left[\hat{\beta}, \hat{\alpha}^\dagger\right] = \left[\hat{\alpha}, \hat{\beta}\right] = \left[\hat{\alpha}^\dagger, \hat{\beta}^\dagger\right] = 0. \tag{2.79}$$

From these commutation relations, the condition for the coefficients follows

$$u^2 - v^2 = 1, \tag{2.80}$$

which can be satisfied by choosing

$$u = \cosh t, \quad v = \sinh t. \tag{2.81}$$

Substituting the transformation into (2.73) yields

$$\begin{aligned} \hat{h} = {} & 2v^2\epsilon_0 - 2uv\epsilon_1 \\ & + \left[\epsilon_0(u^2+v^2) - 2uv\epsilon_1\right](\hat{\alpha}^\dagger\hat{\alpha} + \hat{\beta}^\dagger\hat{\beta}) \\ & + \left[\epsilon_1(u^2+v^2) - 2uv\epsilon_0\right](\hat{\alpha}\hat{\beta} + \hat{\beta}^\dagger\hat{\alpha}^\dagger). \end{aligned} \tag{2.82}$$

To make the Hamiltonian diagonal, we choose u and v such that the $\hat{\alpha}\hat{\beta} + \hat{\beta}^\dagger\hat{\alpha}^\dagger$ term vanishes, which imposes the condition

$$\epsilon_1(u^2+v^2) - 2uv\epsilon_0 = 0. \tag{2.83}$$

Using the expressions (2.81) gives

$$\epsilon_1(\cosh^2 t + \sinh^2 t) - 2\epsilon_0 \sinh t \cosh t = 0, \tag{2.84}$$

from which it follows

$$\tanh 2t = \frac{\epsilon_1}{\epsilon_0}. \tag{2.85}$$

The relations (2.81) then yield

$$u^2 = \frac{1}{2}\left(\frac{\epsilon_0}{\epsilon} + 1\right), \tag{2.86}$$

and

$$v^2 = \frac{1}{2}\left(\frac{\epsilon_0}{\epsilon} - 1\right), \tag{2.87}$$

with

$$\epsilon = \sqrt{\epsilon_0^2 - \epsilon_1^2}. \tag{2.88}$$

Thus, the final diagonalization of (2.73) is

$$\hat{h} = \epsilon(\hat{\alpha}^\dagger\hat{\alpha} + \hat{\beta}^\dagger\hat{\beta}) + \epsilon - \epsilon_0, \tag{2.89}$$

with a negative ground state energy given by $E_0 = \epsilon - \epsilon_0$. The operators $\hat{\alpha}^\dagger$ and $\hat{\beta}^\dagger$ create bosonic excitations that have energy ϵ. The system is stable if ϵ is real. On the other hand, $|\epsilon_1| > |\epsilon_0|$ implies imaginary excitation energy and an unstable system.

2.3.4 Lee-Huang-Yang energy

Returning to the study of Bose gases, the Hamiltonian (2.72) is of the form (2.73), with $\hat{a} = \hat{a}_{\vec{p}}$ and $\hat{b} = \hat{a}_{-\vec{p}}$. By defining $\hat{\alpha} = \hat{\alpha}_{\vec{p}}$ and $\hat{\beta} = \hat{\alpha}_{-\vec{p}}$, equation (2.72) can be rewritten as

$$\hat{\mathscr{H}} = \frac{1}{2}gN\rho\left(1 + \frac{g}{V}\sum_{\vec{p}\neq 0}\frac{m}{p^2}\right) + \sum_{\vec{p}\neq 0}\epsilon(p)\hat{\alpha}_{\vec{p}}^\dagger\hat{\alpha}_{\vec{p}} - \frac{1}{2}\sum_{\vec{p}\neq 0}\left(\frac{p^2}{2m} + g\rho - \epsilon(p)\right), \tag{2.90}$$

where

$$\epsilon(p) = \sqrt{\left(\frac{p^2}{2m} + g\rho\right)^2 - (g\rho)^2} = \sqrt{\left(\frac{p^2}{2m}\right)^2 + \frac{g\rho}{m}p^2}. \tag{2.91}$$

Equation (2.91) can be written as

$$\epsilon(p) = \frac{p}{2m}\sqrt{p^2 + (2mc)^2}, \tag{2.92}$$

where $c = \sqrt{g\rho/m}$ is the sound velocity. Equation (2.92) is the Bogoliubov dispersion relation for elementary excitations.

The Hamiltonian above can be written more neatly as

$$\hat{\mathscr{H}} = E_0 + \sum_{\vec{p}\neq 0}\epsilon(p)\hat{\alpha}_{\vec{p}}^\dagger\hat{\alpha}_{\vec{p}}, \tag{2.93}$$

where the ground state energy is given by

$$\begin{aligned} E_0 &= \frac{1}{2}gN\rho\left(1 + \frac{g}{V}\sum_{\vec{p}\neq 0}\frac{m}{p^2}\right) - \frac{1}{2}\sum_{\vec{p}\neq 0}\left(\frac{p^2}{2m} + g\rho - \epsilon(p)\right) \\ &= \frac{1}{2}gN\rho + \frac{1}{2}\sum_{\vec{p}\neq 0}\left[\epsilon(p) - g\rho - \frac{p^2}{2m} + m\left(\frac{g\rho}{p^2}\right)^2\right], \end{aligned} \tag{2.94}$$

and it corresponds to a vacuum state of quasi-particles created by $\hat{\alpha}^{\dagger}_{\vec{p}}$, for $\vec{p} \neq 0$.

The ground state energy can be calculated by replacing a sum with an integral and observing that only values $p \approx \sqrt{mg\rho}$ have meaningful contributions. The result was calculated by Lee, Huang, and Yang in [16]

$$E_0 = \frac{1}{2} gN\rho \left[1 + \frac{128}{15\sqrt{\pi}} \left(\rho a^3 \right)^{\frac{1}{2}} \right]. \tag{2.95}$$

The chemical potential $\mu = \partial E_0 / \partial N$ is simply given by

$$\mu = g\rho \left[1 + \frac{32}{3\sqrt{\pi}} \left(\rho a^3 \right)^{\frac{1}{2}} \right]. \tag{2.96}$$

The Bogoliubov spectrum (2.92) exhibits distinct behaviors in the long and short wavelength limits. When $p \gg mc$, the excitations behave like free particles, with

$$\epsilon(\vec{p}) \approx \frac{p^2}{2m}. \tag{2.97}$$

In the long wavelength limit, where $p \ll mc$, the excitation spectrum takes the form of acoustic waves,

$$\epsilon(\vec{p}) \approx cp, \tag{2.98}$$

where c is the sound velocity, given by

$$c = \sqrt{\frac{g\rho}{m}}. \tag{2.99}$$

3 Basic theory of Bose-Bose mixtures and Quantum Droplets

When different species of bosons are mixed, also called components, both intraspecies and interspecies interactions need to be considered. Intraspecies interactions can be treated on their own with aformentioned theory, i.e. mean-field with Lee-Huang-Yang corrections (MF+LHY). Interspecies interactions are usually treated only in the mean field regime (MF). For this discussion, density functional theory approach is used. This discussion is primarily based on [36] and [41].

3.1 Mean-field theory of Bose-Bose mixtures

As a first consideration, only MF interactions will be considered. The energy functional of a two-component (species) mixture reads

$$\begin{aligned} E = &\sum_i \int \mathrm{d}\vec{r} \left[\frac{\hbar^2}{2m_i} |\nabla \psi_i(\vec{r})|^2 + V_{i,\,\text{ext.}}(\vec{r}) |\psi_i(\vec{r})|^2 \right] \\ &+ \frac{1}{2} \sum_{i,j} g_{ij} \int \mathrm{d}\vec{r} \, |\psi_i(\vec{r})|^2 |\psi_j(\vec{r})|^2. \end{aligned} \tag{3.1}$$

where $\psi_i(\vec{r})$, $i = 1, 2$, are order parameters - wave functions - of the components, $V_{i,\,\text{ext.}}(\vec{r})$ is the external potential acting on the i-th component, and coupling constants are $g_{ii} = 4\pi\hbar^2 a_{11}/m_i$, $g_{12} = g_{21} = 2\pi\hbar^2 a_{12}/m_r$, with m_r being reduced mass and a_{ij} are s-wave scattering lengths. Coupling constant g_{ii} characterizes the intraspecies interaction between atoms of the i-th component, while g_{12} characterizes the interspecies potential. Densities are analogously to a single-component BEC given by $\rho_i(\vec{r}) = |\psi_i(\vec{r})|^2$.

The time evolution of the mixtures is governed by the coupled Gross-Pitaevskii equations, which can be derived from the variational principle within the framework of Density Functional Theory (DFT) as

$$i\hbar \frac{\partial \psi_i}{\partial t} = \frac{\delta E}{\delta \psi_i^*}, \tag{3.2}$$

where $i = 1, 2$. The coupled Gross-Pitaevskii Equations (GPEs) are given by

$$i\hbar \frac{\partial \psi_i(\vec{r}, t)}{\partial t} = \left[-\frac{\hbar^2}{2m} \nabla^2 + V_{i,\,\text{ext.}} + g_{ii} |\psi_i(\vec{r}, t)|^2 + g_{ij} |\psi_j(\vec{r}, t)|^2 \right] \psi_i(\vec{r}, t). \tag{3.3}$$

Mixtures can exist in two different configurations:

a) **Uniform mixture:** In this configuration, the wave functions overlap, and the two components mix within the volume V. The mean-field (MF) energy for this case is given

by:

$$E_{\text{uniform}} = \frac{1}{2} g_{11} \frac{N_1^2}{V} + \frac{1}{2} g_{22} \frac{N_2^2}{V} + g_{12} \frac{N_1 N_2}{V}. \tag{3.4}$$

b) **Phase-separated configuration:** In this configuration, the wave functions do not overlap. One can visualize this as two blobs next to each other, or with one component forming a ring around the other. Each component occupies its own volume V_i. The MF energy for this case is given by:

$$E_{\text{phase-separated}} = \frac{1}{2} g_{11} \frac{N_1^2}{V_1} + \frac{1}{2} g_{22} \frac{N_2^2}{V_2}. \tag{3.5}$$

In the phase-separated case, mechanical equilibrium is determined by the condition

$$\frac{\partial}{\partial V_1} E_{\text{phase-separated}} = \frac{\partial}{\partial V_2} E_{\text{phase-separated}}, \tag{3.6}$$

which yields

$$g_{11} \left(\frac{N_1}{V_1} \right)^2 = g_{22} \left(\frac{N_2}{V_2} \right)^2. \tag{3.7}$$

This permits rephrasing of equation (3.5) in terms of the total volume, $V = V_1 + V_2$, as

$$E_{\text{phase-separated}} = \frac{1}{2} g_{11} \frac{N_1^2}{V} + \frac{1}{2} g_{22} \frac{N_2^2}{V} + \sqrt{g_{11} g_{22}} \frac{N_1 N_2}{V}. \tag{3.8}$$

From equations (3.4) and (3.8) , the condition needed to avoid phase separation follows:

$$g_{12} < \sqrt{g_{11} g_{22}}. \tag{3.9}$$

In the uniform case, stability against local density fluctuations is determined by the inequality

$$\left(\frac{\partial^2}{\partial N_1^2} E_{\text{uniform}} \right) \left(\frac{\partial^2}{\partial N_2^2} E_{\text{uniform}} \right) > \left(\frac{\partial^2}{\partial N_1 \partial N_2} E_{\text{uniform}} \right)^2, \tag{3.10}$$

which leads to the condition

$$|g_{12}| < \sqrt{g_{11} g_{22}}. \tag{3.11}$$

Mixtures with attractive intraspecies interactions, i.e., $g_{ii} < 0$, are not stable under local density variations, as this leads to the collapse of each component into its own self-bound ground state [41]. Therefore, only mixtures with repulsive intraspecies interactions, $g_{ii} \geq 0$, are stable. In the case of attractive interspecies interactions, $g_{12} < 0$, the condition (3.11) guarantees that perturbing the system does not lead to the formation of a self-bound cluster. Conversely, in the case of repulsive interspecies interactions, $g_{12} > 0$, it ensures that the components do not separate under density perturbations.

For mixtures with $g_{12} < 0$, when $g_{12} = -\sqrt{g_{11}g_{22}}$, the configuration will satisfy

$$\frac{\rho_2}{\rho_1} = \sqrt{\frac{g_{11}}{g_{22}}}, \tag{3.12}$$

which represents the optimal ratio [41]. When $g_{12} > -\sqrt{g_{11}g_{22}}$, the ground state can either be a collapsed state or a dense droplet [37].

3.2 Lee-Huang-Yang energy and Gross-Pitaevskii equation

The previous approach based solely on mean-field (MF) theory breaks down as densities increase and interactions become stronger. Since MF is the lowest-order approximation, a natural remedy to the theory's limitations is found in the first correction: the Lee-Huang-Yang (LHY) term.

Since mixtures are considered within the framework of Density Functional Theory, the LHY correction to the energy density is given by [42]

$$\mathscr{E}_{\text{LHY}}\left[\rho_1, \rho_2\right] = \frac{8}{15\pi^2}\left(\frac{m_1}{\hbar^2}\right)^{\frac{3}{2}}(g_{11}\rho_1)^{\frac{3}{2}} f\left(\frac{m_2}{m_1}, \frac{g_{12}^2}{g_{11}g_{22}}, \frac{g_{22}\rho_2}{g_{11}\rho_1}\right), \tag{3.13}$$

where for the case of $m_1 = m_2$, the function $f(z = 1, u, x)$ is given by

$$f(1, u, x) = \frac{1}{4\sqrt{2}}\sum_{\pm}\left[1 + x \pm \sqrt{(1-x)^2 + 4ux}\right]^{\frac{5}{2}}. \tag{3.14}$$

At the mean-field collapse, where $g_{12}^2 = g_{11}g_{22}$ or $u = 1$, this results in [41]

$$\mathscr{E}_{\text{LHY}}\left[\rho_1, \rho_2\right] = \frac{8}{15\pi^2}\left(\frac{m_1}{\hbar^2}\right)^{\frac{3}{2}}(g_{11}\rho_1)^{\frac{5}{2}}\left(1 + \frac{g_{22}\rho_2}{g_{11}\rho_1}\right)^{\frac{5}{2}}. \tag{3.15}$$

Equation (3.13) was first derived by Larsen in 1964 [43].

Finally, the density functional of a two-component mixture with mean-field (MF) and Lee-Huang-Yang (LHY) interactions reads [35]

$$\begin{aligned} E = &\sum_i \int \mathrm{d}\vec{r}\left[\frac{\hbar^2}{2m_i}|\nabla\psi_i(\vec{r})|^2 + V_{i,\text{ext}}(\vec{r})|\psi_i(\vec{r})|^2\right] \\ &+ \frac{1}{2}\sum_{i,j} g_{ij}\int \mathrm{d}\vec{r}\,|\psi_i(\vec{r})|^2|\psi_j(\vec{r})|^2 \\ &+ \int \mathrm{d}\vec{r}\,\mathscr{E}_{\text{LHY}}\left[\rho_1, \rho_2\right], \end{aligned} \tag{3.16}$$

where $\psi_i(\vec{r})$, $i = 1, 2$, are the order parameters of the components. Since this thesis deals

with potassium mixtures of different hyperfine states, the consideration is further simplified by observing the case of $m_1 = m_2 = m$. From the functional (3.16), one can apply the variational principle, resulting in a coupled pair of generalized Gross-Pitaevskii equations [35]

$$i\hbar\frac{\partial}{\partial t}\psi_i(\vec{r},t) = \left[-\frac{\hbar^2}{2m}\nabla^2 + V_{i,\,\text{ext.}} + g_{ii}|\psi_i(\vec{r},t)|^2 + g_{ij}|\psi_j(\vec{r},t)|^2 + \frac{\partial\mathscr{E}_{\text{LHY}}}{\partial\rho_i}\right]\psi_i(\vec{r},t) = \mathscr{H}_i\psi_i(\vec{r},t). \tag{3.17}$$

3.3 Quantum droplets

Quantum droplets are a type of self-bound state that arises in Bose-Bose mixtures where quantum fluctuations are crucial for system stabilization. Unlike traditional Bose-Einstein condensates, which are generally confined in traps and described by mean-field (MF) interactions, quantum droplets are stabilized through the interplay of quantum effects and mean-field forces.

Dmitri Petrov's paper [22] established a theoretical framework for understanding these droplets. Petrov demonstrated that, under specific conditions, the interplay between quantum fluctuations and mean-field interactions can stabilize a system that would otherwise collapse, i.e., its energy lacks a stable minimum. For attractive mean-field interactions, the energy described by (2.59) does not possess a stable minimum due to its linear dependence on the interactions. However, beyond mean-field effects for repulsive interactions, the Lee-Huang-Yang (LHY) correction introduces a dependence on $\rho^{3/2}$, as shown in equation (2.95), leading to the formation of a stable energy minimum. This stabilization is illustrated in Figure 3. Essentially, the LHY term counterbalances the residual attractive mean-field interaction.

In the droplets that are the focus of this thesis, the balance is maintained by repulsive intraspecies interactions, with $a_{11} > 0$ and $a_{22} > 0$, and attractive interspecies interactions, with $a_{12} < 0$.

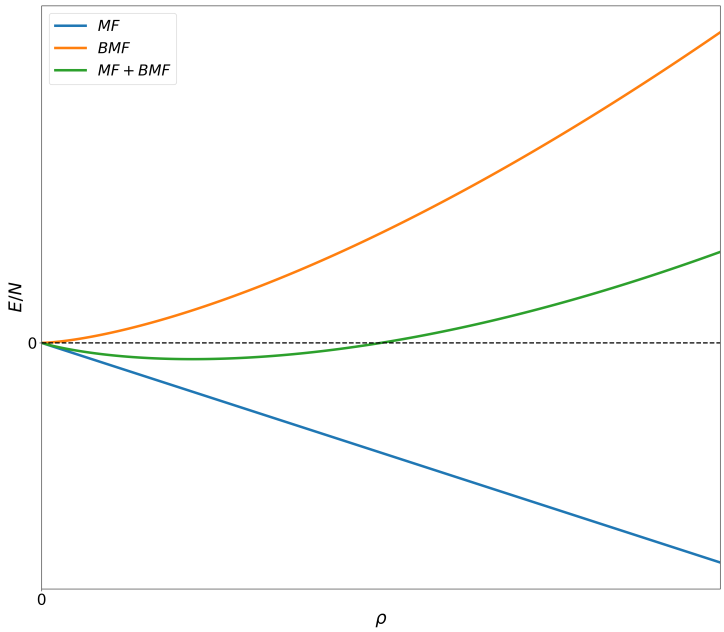

Figure 3: *Graphical illustration of the balance between mean-field (MF) and beyond mean-field (BMF) effects. Together, they define a region where a self-bound droplet may form.*

4 Theory of Superfluids and their Rotation

Superfluids are a peculiar type of fluid which can flow without energy dissipation, exhibiting zero shear viscosity. The most well known example is liquid helium-4 below the λ-point. The phenomenon in helium-4 was discovered by Kapitza [4], Allen, and Misener [5] in 1938, and was theoretically explained by Landau [8] in 1941. Landau found the criteria for excitation spectrum of a fluid which result in motion without dissipation. This chapter focuses on criterion of superfluidity and the rotational properties of superfluids. The discussion is based on Pitaevskii's and Stringari's book [36]

4.1 Basic theory of Superfluidity: Landau's criterion

In an ordinary fluid, flowing particles scatter on imperfections in the system, resulting in energy dissipation. This is not the case in superfluids, which can be understood by observing the acoustic excitation spectrum. Crucial to Landau's explanation is classical relativity, specifically Galilean transformations of energy and momentum.

Consider a uniform fluid at $T = 0$ flowing through a pipe in two reference frames:

a) The rest frame of the fluid S, where the fluid has energy $E = E_0 + \epsilon(\vec{p})$, with E_0 being the ground state energy and $\epsilon(\vec{p})$ the energy of an excitation with momentum $\vec{p}$. Here, $\vec{p}$ represents the momentum carried by the fluid.

b) The rest frame of the pipe S', moving with velocity $-\vec{v}$ relative to S, in which the fluid has velocity $\vec{v}$. In this frame, the fluid's momentum and energy are given by:

$$\vec{p'} = \vec{p} + M\vec{v}, \tag{4.1}$$

and

$$E' = E_0 + \epsilon(\vec{p}) + \vec{p} \cdot \vec{v} + \frac{Mv^2}{2}, \tag{4.2}$$

where M is the total mass of the fluid.

In the system S', the appearance of an excitation in a fluid that is otherwise in the ground state changes the momentum by $\vec{p}$ and the energy by $\epsilon(\vec{p}) + \vec{p} \cdot \vec{v}$. This change corresponds to the energy of the elementary excitation. Such excitations occur spontaneously if the excitation reduces the fluid's energy, i.e.,

$$\epsilon(\vec{p}) + \vec{p} \cdot \vec{v} < 0, \tag{4.3}$$

from which follows the condition

$$v > \frac{\epsilon(\vec{p})}{p}. \tag{4.4}$$

If the fluid can transfer momentum to the pipe, this condition guarantees spontaneous

excitations and, consequently, energy dissipation. On the other hand, the condition (4.4) establishes a certain minimum, or critical, velocity v_c,

$$v_c = \min_{\vec{p}} \frac{\epsilon(\vec{p})}{p}, \tag{4.5}$$

such that for $v < v_c$, there will be no spontaneous excitations. This statement,

$$v < v_c = \min_{\vec{p}} \frac{\epsilon(\vec{p})}{p}, \tag{4.6}$$

is Landau's criterion for superfluidity. When this criterion is satisfied, the fluid will exhibit frictionless flow, stable with respect to the creation of elementary excitations, but metastable in the full thermodynamic picture.

In the case of an ideal Bose gas, the dispersion relation $\epsilon(\vec{p}) = \frac{p^2}{2m}$ leads to a critical velocity of zero, meaning that Landau's criterion (4.6) cannot be satisfied. As a result, ideal Bose gases are not superfluid. In contrast, a weakly interacting Bose gas exhibits the Bogoliubov dispersion relation (2.92), which, in the long wavelength limit, allows for a non-zero critical velocity equal to the sound velocity. Specifically, when $\epsilon(p) = cp$, the critical velocity is given by $v_c = c$.

4.2 Hydrodynamics of superfluids

A common way to describe superfluids is by treating them as a mixture of a "normal" fluid and a superfluid, which do not experience friction between them. This approach was employed by Landau in [8]. It is important to note that this model does not imply that the physical system is composed of two distinct fluids; rather, it provides an elegant description of observed phenomena.

At a given temperature, the total fluid density is given by

$$\rho = \rho_s + \rho_n, \tag{4.7}$$

where ρ_s and ρ_n represent the superfluid and normal mass[1] densities, respectively. The ratio ρ_n/ρ is zero at $T = 0$, and as the temperature increases towards a critical value, this ratio approaches unity. At the critical temperature, superfluid behavior disappears. In helium, the critical temperature is associated with the λ-point.

The macroscopic hydrodynamic description of superfluids is based on a set of hydrodynamic equations [8]:

$$\vec{j} = \rho_s \vec{v}_s + \rho_n \vec{v}_n, \tag{4.8}$$

[1]Here ρ denotes mass density rather than number density, as is the case in the rest of this thesis.

$$\frac{\partial \rho}{\partial t} + \nabla \vec{j} = 0, \tag{4.9}$$

$$\frac{\partial \vec{j}}{\partial t} + \sum_k \frac{\partial \Pi_{ik}}{\partial x_k} = 0, \tag{4.10}$$

$$\Pi_{ik} = P\delta_{ik} + \rho_{\mathrm{s}} \vec{v}_{i,\mathrm{s}} \vec{v}_{k,\mathrm{s}} + \rho_{\mathrm{n}} \vec{v}_{i,\mathrm{n}} \vec{v}_{k,\mathrm{n}}, \tag{4.11}$$

$$\frac{\partial \vec{v}_{\mathrm{s}}}{\partial t} = -\nabla \left[\phi + \frac{v_{\mathrm{s}}^2}{2} - \frac{\rho_{\mathrm{n}}}{2\rho} (\vec{v}_{\mathrm{n}} - \vec{v}_{\mathrm{s}})^2 \right], \tag{4.12}$$

$$\frac{\partial s\rho}{\partial t} + \nabla \left(s\rho \vec{v}_{\mathrm{n}} \right) = 0. \tag{4.13}$$

where $\vec{j}$ is the mass density flux, P is the pressure, s is the entropy per unit mass, ϕ is the thermodynamic potential per unit mass, Π_{ik} is the momentum flux density tensor, while $\vec{v}_{\mathrm{n,s}}$ is the velocity field for the normal (superfluid) component with $v_{i,\mathrm{n,s}}$ being i-th component. These equations are analogous to the hydrodynamic equations for ordinary fluids [44], with the key difference being the absence of viscous terms.

At zero temperature, there are no thermal excitations, and the description of the superfluid can be given in terms of the density ρ and the superfluid velocity $\vec{v}_{\mathrm{s}}$. Introducing the order parameter

$$\psi = \sqrt{\rho} e^{iS}, \tag{4.14}$$

where the superfluid velocity is given by

$$\vec{v}_{\mathrm{s}} = \frac{\hbar}{m} \nabla S, \tag{4.15}$$

captures all the relevant variables. The previous set of hydrodynamic equations simplifies to the following two equations:

$$\frac{\partial \rho}{\partial t} + \nabla \cdot \vec{j} = 0, \tag{4.16}$$

$$m \frac{\partial \vec{v}_{\mathrm{s}}}{\partial t} + \nabla \left(\frac{1}{2} m \vec{v}_{\mathrm{s}}^2 + \mu(\rho) \right) = 0. \tag{4.17}$$

Here, $\mu(\rho)$ represents the chemical potential, which depends on the local uniform fluid density. These equations are essentially the continuity equation and the Euler equation for ideal fluids.

4.3 Rotation of Superfluids

An important property of superfluids is that they do not rotate like ordinary fluids; instead, they form quantized vortex lines. The study of rotating condensates is typically conducted in the rotating reference frame, where the energy is given by

$$E_r = E - \vec{\Omega} \cdot \vec{L}, \tag{4.18}$$

where $\vec{\Omega}$ is the angular velocity and $\vec{L}$ is the angular momentum.

Since the phase of the order parameter is a scalar, the velocity field $\vec{v}_\mathrm{s}$, given by (4.15), obeys

$$\nabla \times \vec{v}_\mathrm{s} = 0. \tag{4.19}$$

The order parameter must be a single-valued function at every point in space. Consequently, the phase change around any closed loop must be an integer multiple of 2π. This implies that the circulation Γ is quantized as

$$\Gamma = \oint \mathrm{d}\vec{l} \cdot \vec{v}_\mathrm{s} = 2\pi \frac{\hbar}{m} s, \tag{4.20}$$

where s is an integer.

Consider a superfluid within a cylindrical vessel, with a straight vortex line running along its symmetry axis. The velocity field magnitude of that superfluid follows from (4.20)

$$v_\mathrm{s} = \frac{\hbar}{mr} s, \tag{4.21}$$

where r is the distance from the vortex line. The angular momentum of that superfluid may expressed as

$$L_z = \int \mathrm{d}\vec{r}\, r \rho_\mathrm{s} v_\mathrm{s} = \pi R^2 L \rho_\mathrm{s} \frac{\hbar}{m} s, \tag{4.22}$$

where v_s represents the velocity along streamlines, ρ_s denotes the superfluid density far from the vortex, L is the length of the vessel, and R is its radius. The energy associated with the vortex is primarily kinetic and can be formulated as

$$E_\mathrm{v} = \int_{r_\mathrm{c}}^{R} \mathrm{d}\vec{r} \frac{1}{2} \rho_\mathrm{s} v_\mathrm{s}^2 = L\pi\rho_\mathrm{s} s^2 \left(\frac{\hbar}{m}\right)^2 \ln\left(\frac{R}{r_\mathrm{c}}\right), \tag{4.23}$$

where r_c represents the radius of the vortex core. The critical angular velocity Ω_c required for the existence of a stable vortex is determined by the condition that the change in energy due to rotation equals E_v, hence $E_\mathrm{v} = \Omega_\mathrm{c} L_z$. For $s = 1$ vortices, the critical value is given by

$$\Omega_\mathrm{c} = \frac{E_\mathrm{v}}{L_z} = \frac{\hbar}{mR^2} \ln\left(\frac{R}{r_\mathrm{c}}\right). \tag{4.24}$$

4.4 Bose-Einstein condensate as a superfluid

Bose-Einstein condensates in the absence of external potentials are described by the Hamiltonian

$$\hat{\mathscr{H}} = \int \mathrm{d}\vec{r} \left(\frac{\hbar^2}{2m} \nabla \hat{\Psi}^\dagger(\vec{r},t) \nabla \hat{\Psi}(\vec{r},t) \right) + \frac{1}{2} \int \mathrm{d}\vec{r} \mathrm{d}\vec{r} \, \hat{\Psi}^\dagger(\vec{r'},t) \hat{\Psi}^\dagger(\vec{r},t) V(\vec{r'}-\vec{r}) \hat{\Psi}(\vec{r'},t) \hat{\Psi}(\vec{r},t), \tag{4.25}$$

which is invariant under spatial translations. This, by Noether's theorem, leads to the conservation of momentum. The Galilean transformation of the field operator is given by [36]

$$\hat{\Psi}'(\vec{r},t) = \hat{\Psi}\left(\vec{r} - \vec{v}t, t\right) e^{\frac{i}{\hbar}\left(m\vec{v}\cdot\vec{r} - \frac{1}{2}mv^2 t\right)}, \tag{4.26}$$

where $\vec{v}$ is a constant vector. In the BEC rest frame, the order parameter is

$$\Psi = \sqrt{\rho_0} e^{-\frac{i}{\hbar}\mu t}, \tag{4.27}$$

while in the reference frame where the BEC moves with velocity $\vec{v}$, the order parameter becomes

$$\Psi = \sqrt{\rho} e^{iS} = \sqrt{\rho_0} e^{\frac{i}{\hbar}\left[m\vec{v}\cdot\vec{r} - \left(\frac{1}{2}mv^2 + \mu\right)t\right]}. \tag{4.28}$$

The superfluid velocity field is given in terms of the phase S as

$$\vec{v}_\mathrm{s} = \frac{\hbar}{m} \nabla S. \tag{4.29}$$

Since the energy in the rotating frame is given by (4.18), the Gross-Pitaevskii equation in the rotating frame is expressed as

$$i\hbar \frac{\partial}{\partial t} \psi_i(\vec{r},t) = \left[\hat{\mathscr{H}}_i - \vec{\Omega} \cdot \hat{\vec{L}} \right] \psi_i(\vec{r},t), \tag{4.30}$$

where $\hat{\vec{L}}$ is the angular momentum operator. It is customary to choose the rotation axis to be the z-axis, i.e., $\vec{\Omega} = \Omega \vec{e}_z$, in which case the Hamiltonian in (4.30) simplifies to

$$i\hbar \frac{\partial}{\partial t} \psi_i(\vec{r},t) = \left[\hat{\mathscr{H}}_i - \Omega \hat{L}_z \right] \psi_i(\vec{r},t), \tag{4.31}$$

where

$$\hat{L}_z = \hat{x}\hat{p}_y - \hat{y}\hat{p}_x = -i\hbar \left(\hat{x} \frac{\partial}{\partial y} - \hat{y} \frac{\partial}{\partial x} \right). \tag{4.32}$$

5 Numerical method for solving the equations

The Hamiltonian of interest for our systems is

$$\mathscr{H} = \frac{1}{2m}\left(p_x^2 + p_y^2 + p_z^2\right) + \frac{1}{2}m\omega_z^2 z^2 + V_{\text{MF+LHY}} - \Omega\left(xp_y - yp_x\right) . \tag{5.1}$$

Note that in this section the hats on operators will be dropped for simplicity. In order to solve it we will rephrase the Hamiltonian as

$$\mathscr{H} = \frac{1}{2m}\left(p_x^2 + p_y^2 + p_z^2\right) + \left(\frac{1}{2} - \frac{1}{2}\right) m\omega_{xy}^2\left[(1+\delta)x^2 + (1-\delta)y^2\right] + \frac{1}{2}m\omega_z^2 z^2 + V_{\text{MF+LHY}} - \Omega\left(xp_y - yp_x\right) , \tag{5.2}$$

and split it as

$$\mathscr{H} = \mathscr{H}_{xy} - \frac{1}{2}m\omega_{xy}^2\left[(1+\delta)x^2 + (1-\delta)y^2\right] + \frac{1}{2m}p_z^2 + \frac{1}{2}m\omega_z^2 z^2 + V_{\text{MF+LHY}} . \tag{5.3}$$

In these equations a harmonic potential, with the frequency ω_{xy} and anisotropy δ, was introduced and subsequently subtracted. With this adjustment, the problem becomes solvable using the method developed by Chin and Krotscheck [45].

5.1 Theoretical derivation

To solve the equation given by (5.3) the method of Oktel, and Chin and Krotscheck from [45, 46] will be employed. Starting with the Hamiltonian of the form

$$\mathscr{H}_{xy} = \frac{1}{2m}\left(p_x^2 + p_y^2\right) + \frac{1}{2}m\omega_{xy}^2\left[(1+\delta)x^2 + (1-\delta)y^2\right] - \Omega\left(xp_y - yp_x\right) \tag{5.4}$$

the aim is to arrive at at the Hamiltonian

$$\mathscr{H}_{xy} = \frac{1}{2}\left[P_1^2 + P_2^2 + \Omega_1^2 Q_1^2 + \Omega_2^2 Q_2^2\right] \tag{5.5}$$

using a canonical transformation.

Firstly, the Hamiltonian (5.4) is to be expressed in units of $\hbar^2/(ma_{11}^2)$, from which naturally follow the definitions for coordinates $x' = x/a_{11}$ and momenta $p'_x = -(i/\hbar)p_x = -i\frac{\partial}{\partial x'} = -ia_{11}\frac{\partial}{\partial x}$. Momentum can also then be easily expressed in reciprocal space as $p'_x = k'_x$. Hamiltonian in the new units is

$$\mathscr{H}'_{xy} = \frac{1}{2}\left(p_x'^2 + p_y'^2\right) + \frac{1}{2a_{xy}'^4}\left[(1+\delta)x^2 + (1-\delta)y^2\right] - f_\Omega\Omega\left(x'p'_y - y'p'_x\right) , \tag{5.6}$$

where $a_{xy}'^2 = a_{xy}^2/a_{11}^2 = \frac{\hbar}{m\omega_{xy}a_{11}^2}$ and $f_\Omega = \frac{ma_{11}^2}{\hbar}$.

Next we define $\tilde{x} = x/a_{xy}^2$ and $\tilde{\Omega} = f_\Omega \Omega$ so that the Hamiltonian becomes

$$\mathscr{H}_{xy} = \frac{1}{2}\left(p_x^2 + p_y^2\right) + \frac{1}{2}\left[(1+\delta)\tilde{x}^2 + (1-\delta)\tilde{y}^2\right] - \tilde{\Omega}\left(xp_y - yp_x\right) . \tag{5.7}$$

Now we can introduce the following linear canonical transformation

$$Q_1 = \alpha_1 \left[\cos(\phi)\tilde{x} - \sin(\phi)p_y\right] , \tag{5.8}$$

$$P_1 = \frac{1}{\alpha_1}\left[\sin(\phi)\tilde{y} + \cos(\phi)p_x\right] , \tag{5.9}$$

$$Q_2 = \alpha_2 \left[\cos(\phi)\tilde{y} - \sin(\phi)p_x\right] , \tag{5.10}$$

$$P_2 = \frac{1}{\alpha_2}\left[\sin(\phi)\tilde{x} + \cos(\phi)p_y\right] , \tag{5.11}$$

with a condition that $\tan(2\phi) = 2\tilde{\Omega}/\delta$. It can be shown that the commutator is

$$[Q_j, P_k] = \frac{i}{a_{xy}^2}\delta_{jk} . \tag{5.12}$$

Looking at pairs Q_1 and P_2, as well as Q_2 and P_1, old canonical variables can be expressed using new ones as

$$\tilde{x} = \frac{\cos(\phi)}{\alpha_1}Q_1 + \sin(\phi)\alpha_2 P_2 , \tag{5.13}$$

$$p_x = \cos(\phi)\alpha_1 P_1 - \frac{\sin(\phi)}{\alpha_2}Q_2 , \tag{5.14}$$

$$\tilde{y} = \frac{\cos(\phi)}{\alpha_2}Q_2 + \sin(\phi)\alpha_1 P_1 , \tag{5.15}$$

$$p_y = \cos(\phi)\alpha_2 P_2 - \frac{\sin(\phi)}{\alpha_1}Q_1 . \tag{5.16}$$

Plugging those back into (5.7) yields

$$\begin{aligned}\mathscr{H}_{xy} =&\frac{1}{2}\alpha_1^2 P_1^2\left[\cos^2(\phi)+\sin^2(\phi)(1-\delta)+\tilde{\Omega}\sin(2\phi)\right]\\ &+\frac{1}{2}\alpha_2^2 P_2^2\left[\cos^2(\phi)+\sin^2(\phi)(1+\delta)-\tilde{\Omega}\sin(2\phi)\right]\\ &+\frac{1}{2\alpha_1^2}Q_1^2\left[\sin^2(\phi)+\cos^2(\phi)(1+\delta)+\tilde{\Omega}\sin(2\phi)\right]\\ &+\frac{1}{2\alpha_2^2}Q_2^2\left[\sin^2(\phi)+\cos^2(\phi)(1-\delta)-\tilde{\Omega}\sin(2\phi)\right]\\ &-\frac{\sin(2\phi)}{2}\left[\frac{\alpha_1}{\alpha_2}P_1Q_2+\frac{\alpha_2}{\alpha_1}P_2Q_1\right]\\ &+\frac{\sin(2\phi)}{2}\left[(1+\delta)\frac{\alpha_2}{\alpha_1}P_2Q_1+(1-\delta)\frac{\alpha_1}{\alpha_2}P_1Q_2\right]\\ &+\cos(2\phi)\tilde{\Omega}\left[\frac{\alpha_1}{\alpha_2}P_1Q_2-\frac{\alpha_2}{\alpha_1}P_2Q_1\right].\end{aligned} \tag{5.17}$$

From (5.17), keeping in mind the goal of reaching (5.5), follow demands that

$$\alpha_1^2\left[\cos^2(\phi)+\sin^2(\phi)(1-\delta)+\tilde{\Omega}\sin(2\phi)\right]=1\,, \tag{5.18}$$

$$\alpha_2^2\left[\cos^2(\phi)+\sin^2(\phi)(1+\delta)-\tilde{\Omega}\sin(2\phi)\right]=1\,, \tag{5.19}$$

$$\frac{1}{\alpha_1^2}\left[\sin^2(\phi)+\cos^2(\phi)(1+\delta)+\tilde{\Omega}\sin(2\phi)\right]=\Omega_1^2\,, \tag{5.20}$$

$$\frac{1}{\alpha_2^2}\left[\sin^2(\phi)+\cos^2(\phi)(1-\delta)-\tilde{\Omega}\sin(2\phi)\right]=\Omega_2^2\,, \tag{5.21}$$

and

$$\begin{aligned}&-\frac{\sin(2\phi)}{2}\left[\frac{\alpha_1}{\alpha_2}P_1Q_2+\frac{\alpha_2}{\alpha_1}P_2Q_1\right]\\ &+\frac{\sin(2\phi)}{2}\left[(1+\delta)\frac{\alpha_2}{\alpha_1}P_2Q_1+(1-\delta)\frac{\alpha_1}{\alpha_2}P_1Q_2\right]\\ &+\cos(2\phi)\tilde{\Omega}\left[\frac{\alpha_1}{\alpha_2}P_1Q_2-\frac{\alpha_2}{\alpha_1}P_2Q_1\right]=0\,.\end{aligned} \tag{5.22}$$

With the earlier condition that $\tan(2\phi)=2\tilde{\Omega}/\delta$ (5.22) holds while others simplify to give

$$\frac{1}{\alpha_1^2}=1-\frac{\delta}{2}+\frac{1}{2}\sqrt{\delta^2+4\tilde{\Omega}^2}\,, \tag{5.23}$$

$$\frac{1}{\alpha_2^2}=1+\frac{\delta}{2}-\frac{1}{2}\sqrt{\delta^2+4\tilde{\Omega}^2}\,, \tag{5.24}$$

$$\Omega_1^2=\frac{1}{\alpha_1^2}\left(1+\frac{\delta}{2}+\frac{1}{2}\sqrt{\delta^2+4\tilde{\Omega}^2}\right)\,, \tag{5.25}$$

and finally

$$\Omega_2^2 = \frac{1}{\alpha_2^2}\left(1 - \frac{\delta}{2} - \frac{1}{2}\sqrt{\delta^2 + 4\tilde{\Omega}^2}\right) . \tag{5.26}$$

These expressions coincide with those presented in Oktel's work [46], as well as those found in the paper by Chin and Krotscheck [45].

5.2 Algorithmic implementation

The aim is to solve the equation

$$i\frac{\partial}{\partial t}\psi = \mathscr{H}\psi\,, \tag{5.27}$$

with the Hamiltonian

$$\mathscr{H} = \mathscr{H}_{xy} + \mathscr{V}\,, \tag{5.28}$$

with $\mathscr{H}_{xy}$ being given by (5.6), and

$$\mathscr{V} = -\frac{1}{2a_{xy}'^4}\left[(1+\delta)x^2 + (1-\delta)y^2\right] + \frac{1}{2}p_z^2 + \frac{1}{2a_z'^4}z^2 + V'_{\text{MF+LHY}}\,. \tag{5.29}$$

We use a second order algorithm in imaginary time $\tau = it$ from [45]

$$\begin{aligned}\psi(\tau+\Delta\tau) = &\exp\left(-\frac{1}{6}\Delta\tau\mathscr{V}\right)\exp\left(-\frac{1}{2}\Delta\tau\mathscr{H}_{xy}\right)\\ &\times\exp\left(-\frac{2}{3}\Delta\tau\mathscr{V}\right)\exp\left(-\frac{1}{2}\Delta\tau\mathscr{H}_{xy}\right)\exp\left(-\frac{1}{6}\Delta\tau\mathscr{V}\right)\psi(\tau)\,.\end{aligned} \tag{5.30}$$

Evolution with $\mathscr{H}_{xy}$ is done in steps [45]:

a) Starting from $\psi(x,y,z)$ we compute $\psi(p_x,y,z)$ using a forward one dimensional fast Fourier transform (FFT) and multiply the result with $\exp\left[-\frac{\Delta\tau}{8}\left(P_1^2 + \Omega_2^2 Q_2^2\right)\right]$.

b) We compute $\psi(x,p_y,z)$ using a two dimensional FFT and multiply the result with $\exp\left[-\frac{\Delta\tau}{4}\left(\Omega_1^2 Q_1^2 + P_2^2\right)\right]$.

c) We compute $\psi(p_x,y,z)$ using an inverse two dimensional FFT and multiply the result with $\exp\left[-\frac{\Delta\tau}{8}\left(P_1^2 + \Omega_2^2 Q_2^2\right)\right]$.

d) We compute $\psi(x,y,z)$ using the backward one dimensional inverse FFT.

The algorithm remains stable for $\Omega/\omega_{xy} < \sqrt{1-\delta}$, beyond which the harmonic trap potential introduced in (5.2) becomes unstable [45]. While the Gross-Pitaevskii equation can support "overcritical" rotation under sufficiently strong interaction terms, a detailed discussion of this is outside the scope of this thesis.

5.3 Angular momentum calculation

The angular momentum operator $\hat{L}_z$ is given by

$$\hat{L}_z = -i\hbar \left(x\frac{\partial}{\partial y} - y\frac{\partial}{\partial x} \right), \tag{5.31}$$

and its expectation value is

$$\left\langle \hat{L}_z \right\rangle = \langle \psi | \hat{L}_z | \psi \rangle = \int \mathrm{d}\vec{r}\, \psi^*(\vec{r}) \hat{L}_z \psi(\vec{r}). \tag{5.32}$$

The simplest way to calculate this is by first computing $\hat{L}_z\psi(\vec{r})$ using a numerical derivative, multiplying by $\psi^*(\vec{r})$, and then integrating the result. To perform the numerical differentiation, one can use finite difference approximations. The approximation with second-order accuracy is

$$f'(x) \approx \frac{f(x+h) - f(x-h)}{2h} + \mathscr{O}(h^2), \tag{5.33}$$

and the approximation with fourth-order accuracy is

$$f'(x) \approx \frac{-f(x+2h) + 8f(x+h) - 8f(x-h) + f(x-2h)}{12h} + \mathscr{O}(h^4). \tag{5.34}$$

Another approach to this calculation is through Fourier transformations. Specifically, the use of the the following expression:

$$\left\langle \hat{L}_z \right\rangle = \frac{1}{\mathscr{N}_{x,p_y}} \int \mathrm{d}x \mathrm{d}p_y\, x p_y |\psi(x, p_y, z)|^2 + \frac{1}{\mathscr{N}_{p_x,y}} \int \mathrm{d}p_x \mathrm{d}y\, y p_x |\psi(p_x, y, z)|^2, \tag{5.35}$$

where the normalization factor $\mathscr{N}_{r_i,p_j}$ is given by

$$\mathscr{N}_{r_i,p_j} = \frac{1}{N} \int \mathrm{d}r_i \mathrm{d}p_j\, |\psi(r_i, p_j)|^2. \tag{5.36}$$

6 Non-rotating self-bound droplets

The quantum droplets under consideration are binary mixtures of potassium-39 in a magnetic field of strength 56.337 G, confined along the z-axis. The confinement potential is harmonic, given by $m\omega_z^2 z^2/2$, where $\omega_z = \hbar/(ma_z^2)$. The oscillator length is $a_z = f \times 0.639\,\mu$m. The scattering lengths for the system are

$$a_{11} = 66.619\,a_0, \quad a_{22} = 34.369\,a_0, \quad a_{12} = -53.386\,a_0, \tag{6.1}$$

where a_0 is the Bohr radius. The optimal ratio of atom numbers is maintained, although it is not strictly necessary

$$\frac{N_1}{N_2} = \sqrt{\frac{a_{22}}{a_{11}}}. \tag{6.2}$$

Since $a_{11} > a_{22}$, the more numerous component is N_2.

The equation we are solving is an extended Gross-Pitaevskii equation in the rotating reference frame

$$i\hbar\frac{\partial}{\partial t}\psi_i(\vec{r},t) = \left[-\frac{\hbar^2}{2m}\nabla^2 + V_i + g_{ii}|\psi_i(\vec{r},t)|^2 + g_{ij}|\psi_j(\vec{r},t)|^2 + \frac{\partial\mathscr{E}_{\text{LHY}}}{\partial\rho_i} - \Omega\hat{L}_z\right]\psi_i(\vec{r},t). \tag{6.3}$$

Taking $\Omega = 0$ reduces the problem to a non-rotating one. For the harmonic potential in the xy-plane, we take $a_{xy} = 2\,\mu$m.

Starting from a broad Gaussian for the wave functions, the aim is to find the ground state energy and profile. The spatial grid used is $128 \times 128 \times 64$, with the lower discretization along the z-axis being feasible due to confinement. The size of the simulation box is typically $10000 \times 10000 \times 1280$ in a_{11} units, further adjusted where necessary according to the size of the system. This setup provides a good resolution for larger systems while maintaining reasonable simulation duration. The simulation time is generally set to 10^6 inverse energy units for non-rotating droplets, with a time step of 200. This time step was choosen as a it offers a balance between accuracy and computational time. Figure 4 shows that the total simulation time is sufficiently long for the energy to equilibrate. Notably, regardless of the chosen time step, a stable energy value is reached after approximately the same total time, $t = N_{\text{steps}} \times dt$. The dependence of E on dt is quadratic, as expected. Table 1 summarizes the simulation durations for total simulation time $t = 10^6$ with different different time steps. The smaller dt necessitates a larger number of steps to reach the same total time, resulting in longer durations for the calculations.

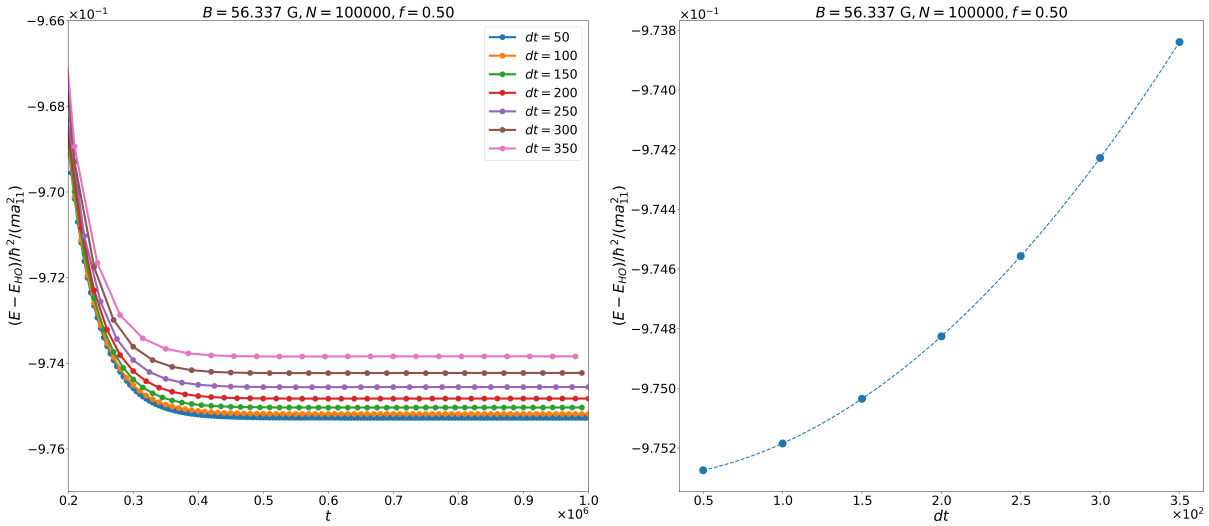

(a) *Self-bound energy during the simulation with different time steps. Notably, each choice results in a stable energy after approximately the same total time, t.*

(b) *Final values for self-bound energy during the simulation for different time steps. Dashed line is a second degree polynomial fit.*

Figure 4: *Self-bound energy for a system of $N = 1 \times 10^5$ atoms at confinement $f = 0.5$. The total simulation time, $t = N_{steps} \times dt = 10^6$ is consistent across all time step choices. Observe the quadratic dependence of E on dt.*

Time step dt	50	100	150	200	250	300	350
Duration in hours	8.57	4.34	2.66	2.24	1.83	1.55	1.35

Table 1: *Simulation durations for different time steps. The total simulation time, $t = N_{steps} \times dt = 10^6$, is consistent across all time step choices.*

The results generally agree well with those in [34], where the single equation for optimal density was solved without the aforementioned transformations. The comparison of energies is shown in Table 2, while the comparison of density profiles can be seen in Figure 5 for the case of 10^5 atoms at $f = 0.50$.

The energy plot for a droplet of 10^5 atoms with a squeezing factor of 0.5 in Figure 6 confirms the convergence of the results, while the angular momentum oscillations around zero align with the expectations of numerical noise. Figures 7 and 8 show the density profiles for this droplet. In the center of the system, the droplet begins to reach a constant bulk density, as expected. The same behavior is observed with 10^6 atoms, as seen in Figures 9 and 10, where one can also observe that additional particles cause the droplet to spread perpendicularly to the squeezing.

When discussing energies, it is useful to subtract the contribution of the squeezing potential

$$E - E_{\text{H.O.}} = E[\psi(\vec{r},t)] - \int \mathrm{d}\vec{r}\,\frac{1}{2}m\omega_z^2 z^2 |\psi(\vec{r},t)|^2 = E[\psi(\vec{r},t)] - \frac{\hbar^2}{2ma_z^4}\int \mathrm{d}\vec{r}\, z^2 |\psi(\vec{r},t)|^2, \tag{6.4}$$

which allows for a discussion focused on the self-binding energy resulting from interatomic interactions. Furthermore, examining the energy per particle permits comparisons between

droplets of different sizes.

N	f	E_{paper} $[\hbar^2/(ma_{11}^2)]$	E_{thesis} $[\hbar^2/(ma_{11}^2)]$
15000	0.25	3.539	3.543
25000	0.25	5.869	5.876
50000	0.25	11.681	11.695
70000	0.25	16.324	16.343
20000	0.50	1.092	1.092
50000	0.50	2.613	2.612
100000	0.50	5.110	5.108
200000	0.50	10.062	10.059
20000	0.75	0.444	0.444
50000	0.75	0.966	0.966
100000	0.75	1.789	1.787

Table 2: *Comparison of calculated total energies. E_{paper} are results from [34].*

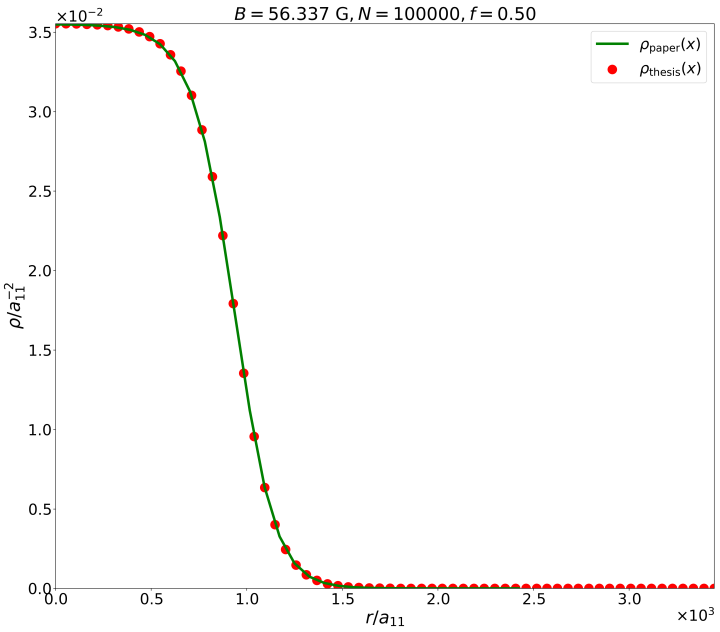

Figure 5: *Integrated total density of the droplet in the xy-plane; comparison of methods. $N = 1 \times 10^5$, $f = 0.5$. ρ_{paper} is the density profile from [34].*

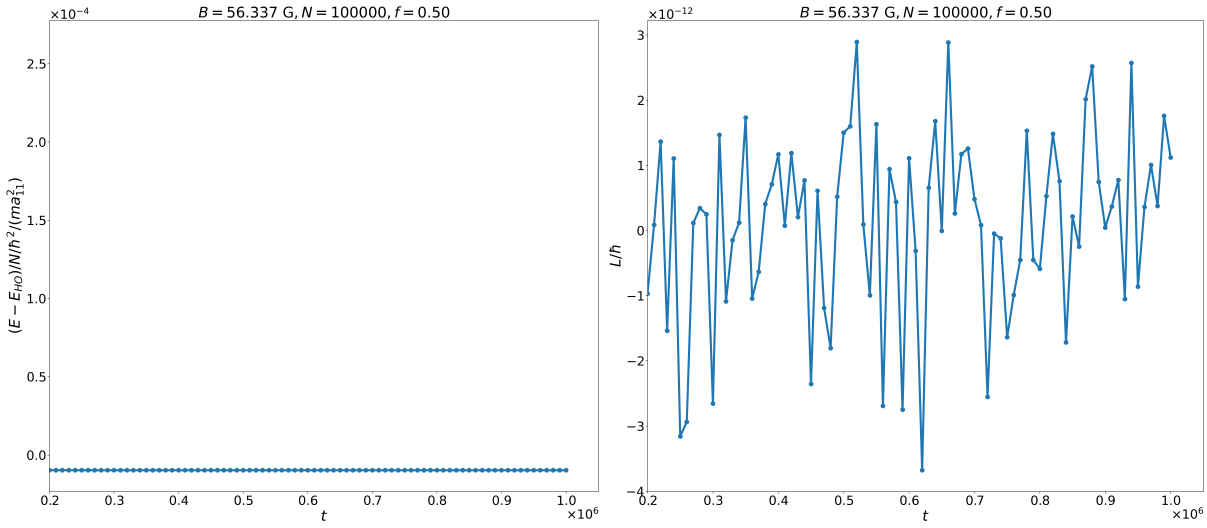

(a) *Energy per particle during the simulation.* **(b)** *Angular momentum during the simulation.*

Figure 6: *Energy and angular momentum per particle during the simulation, showing stabilization of the solution. Droplet with* $N = 1 \times 10^5$ *atoms at confinement* $f = 0.5$.

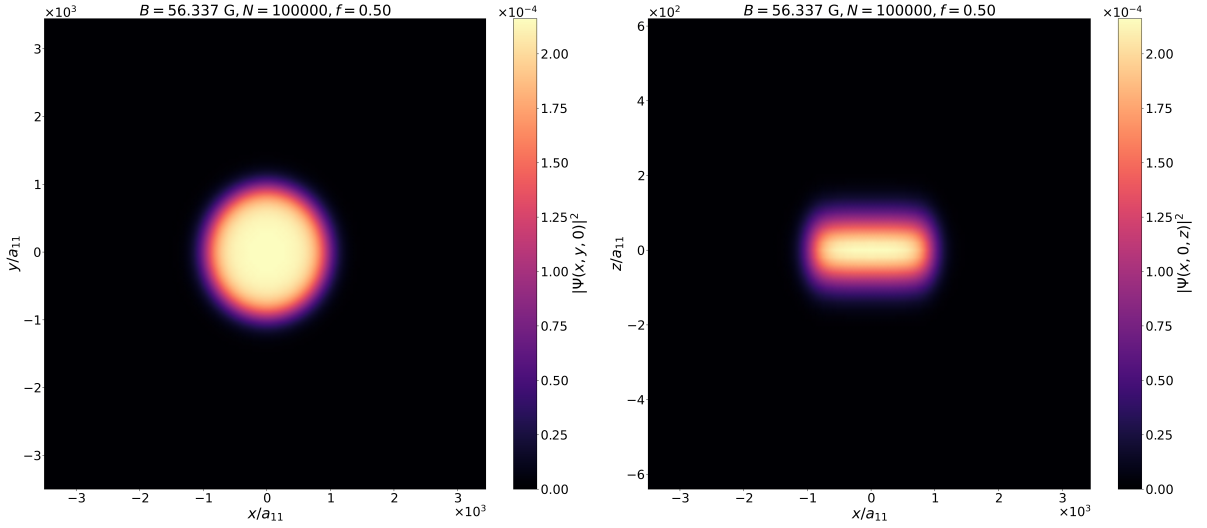

(a) *Total droplet density in the* xy*-plane at* $z = 0$. **(b)** *Total droplet density in the* xz*-plane at* $y = 0$.

Figure 7: *Total droplet density* $\rho = \rho_1 + \rho_2$ *in scattering length units for a drop with* $N = 1 \times 10^5$ *atoms at confinement* $f = 0.5$.

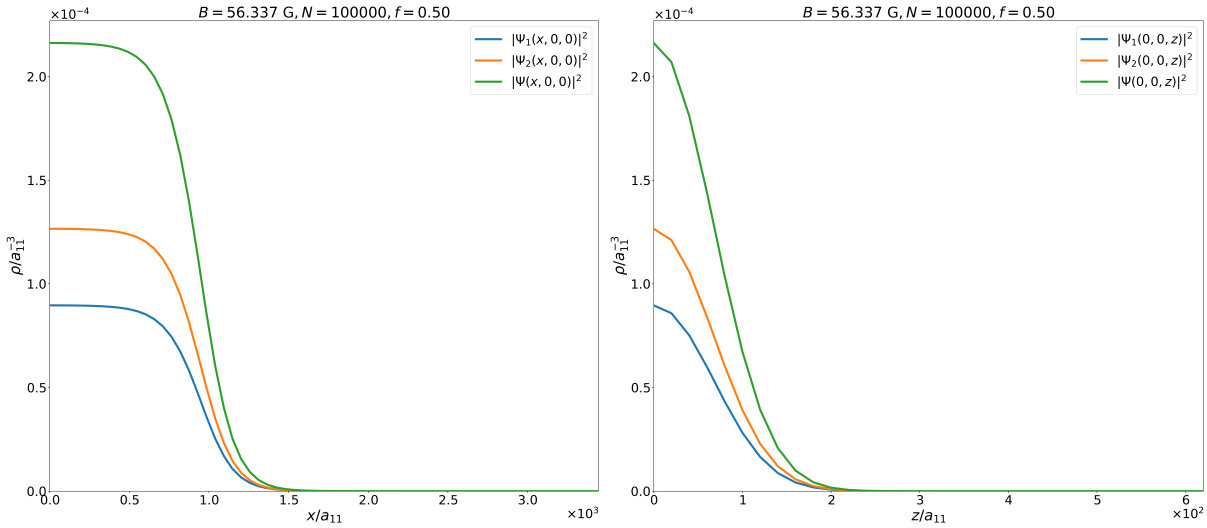

(a) *Total droplet density and component densities along the x-axis in the droplet center.*

(b) *Total droplet density and component densities along the z-axis in the droplet center.*

Figure 8: *Component and total droplet densities in scattering length units for a drop with $N = 1 \times 10^5$ atoms at confinement $f = 0.5$.*

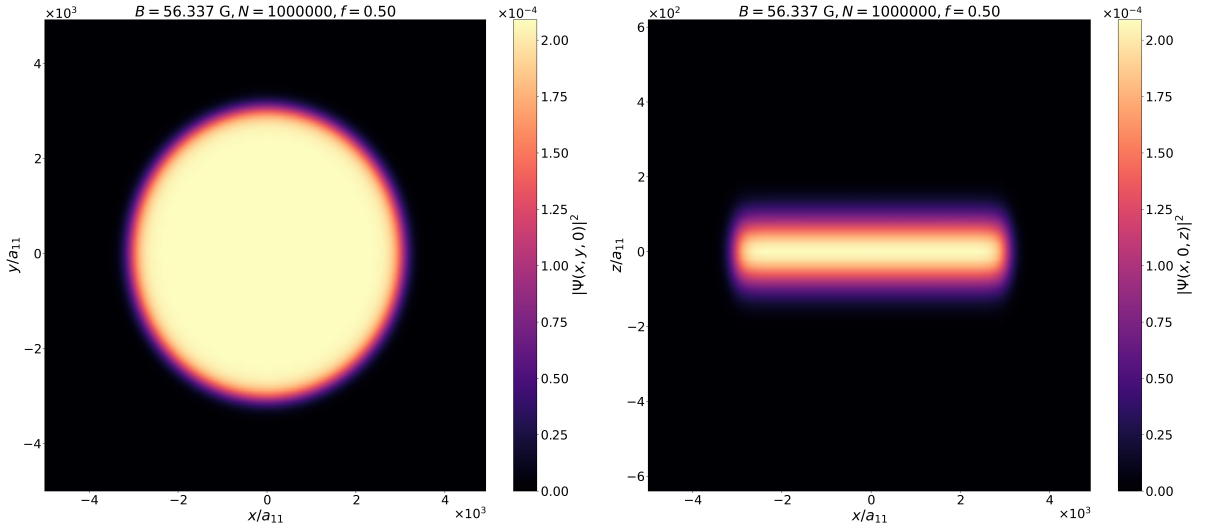

(a) *Total droplet density in the xy-plane at $z = 0$.*

(b) *Total droplet density and component densities along the z-axis in the droplet center.*

Figure 9: *Total droplet density in scattering length units for a drop with $N = 1 \times 10^6$ atoms at confinement $f = 0.5$.*

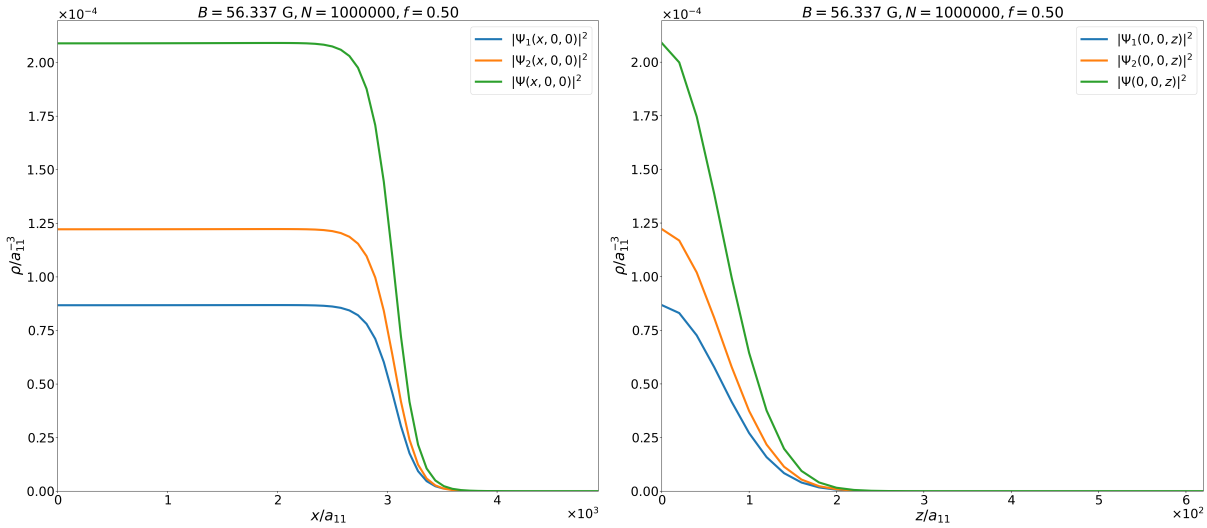

(a) *Total droplet density and component densities along the x-axis in the droplet center.*

(b) *Total droplet density and component densities along the z-axis in the droplet center.*

Figure 10: *Component and total droplet densities in scattering length units for a drop with $N = 1 \times 10^6$ atoms at confinement $f = 0.5$.*

7 Vortices in rotating self-bound droplets

7.1 Angular Momentum

In Section 5.3, various methods for calculating angular momentum were discussed. The results obtained from these methods are compared in Figure 11. Overall, the results are relatively close, with the higher-order derivative method $L_{\text{D: }O(h^4)}$ and the Fourier transform method L_{FT} showing especially close agreement. Between these two, the Fourier transform method is preferred due to its speed, being approximately 13% faster, as illustrated in Table 3.

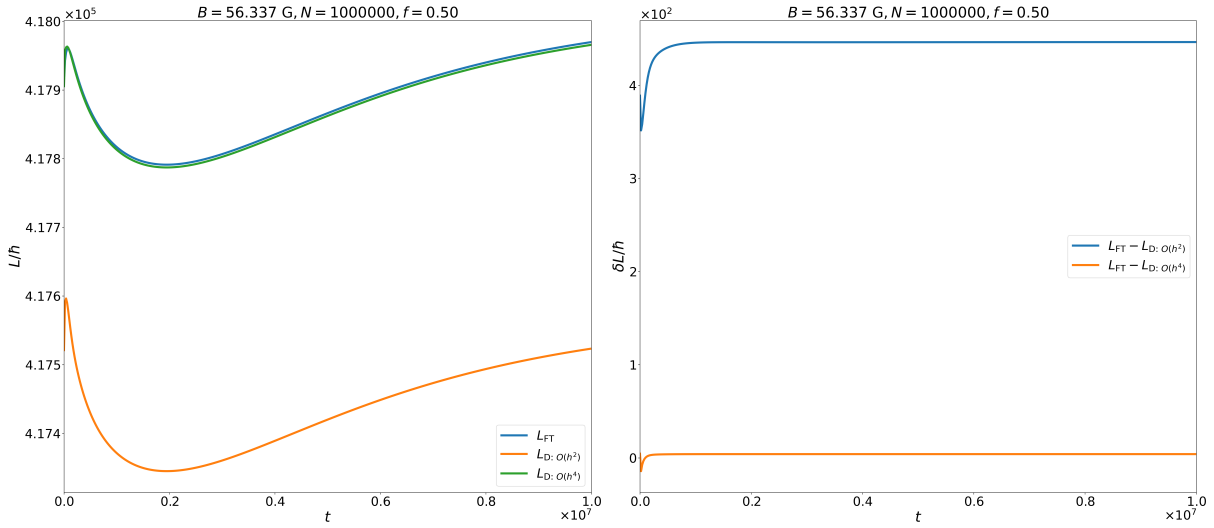

(a) *Comparison of angular momentum values calculated using different methods.*

(b) *Differences between angular momentum values calculated using different methods.*

Figure 11: *Calculation of angular momentum using different methods. The value calculated using Fourier transforms is denoted as L_{FT}, while $L_{D:\,O(h^2)}$ and $L_{D:\,O(h^4)}$ are calculated using numerical differentiation with precisions of $O(h^2)$ and $O(h^4)$, respectively.*

Method	L_{FT}	$L_{\text{D: }O(h^2)}$	$L_{\text{D: }O(h^4)}$
Duration in hours	14.91	16.49	17.25

Table 3: *Simulation durations for different angular momentum calculation methods. Total simulation time is $t = 10^7$, with the time step $dt = 200$.*

7.2 Droplets with vortices

Working with the same potassium-39 atoms and starting from the previous solutions, a vortex is introduced in the center as

$$\psi_j = \psi_{j,\text{no vortex}} \times \exp\left(i l_j \phi\right), \tag{7.1}$$

where $\phi = \arctan\left(\frac{y}{x}\right)$ is the polar angle and l_j being the integer quantum number for the vortex in component j. At the center of the vortex, $\psi_j(0,0,z) = 0$ is set. For all results, the angular velocity is

$$\Omega = 10 \times 2\pi\,\mathrm{s}^{-1}. \tag{7.2}$$

This value is chosen as it is above the critical velocity for vortices (4.24) and should safely accommodate a vortex solution. The time step and discretization are kept the same as in the previous simulations; however, the total simulation time is lengthened to $t = 10^7$ since angular momentum takes longer to fully stabilize. Again, we take $a_{xy} = 2\,\mu$m, for which the critical angular velocity for algorithmic stability works out to $\Omega_\mathrm{c} = 64.59 \times 2\pi\,\mathrm{s}^{-1}$.

Table 4 presents the energy per particle and the angular momentum calculated for several cases involving different particle numbers, confinement, and vortex configurations. A key observation from this data is that the angular momentum per particle of the rotating component is consistently equal to, or just below, $1\hbar$ across all cases. This precise value is particularly evident due to rounding effects; without rounding, the ratio approaches 1. The two cases where the ratio is slightly below 1 exhibited slower convergence due to being on the edge of stability, but the overall trend clearly indicates convergence towards 1. This outcome aligns with theoretical expectations, when considering the presence of a centered vortex [37].

Furthermore, decreasing the confinement factor f (i.e., increasing the squeezing) results in more negative energy, indicating that strongly squeezed configurations are more self-bound. This trend is clearly visible in Figure 12, regardless of the location of the vortices. This behavior could be explained by the larger proportion of the droplet being in the bulk density region under stronger confinement.

Figure 13 presents the same data but grouped in cases of different vortex presence under the same confinement. It is evident that, generally, it is more energetically favorable for the vortex to be present in the less numerous species 1, as opposed to species 2 or both species simultaneously. The presence of the vortex in both species results in the least self-binding, which is intuitively expected. Considering a hydrodynamic approach to vortex energy, as was done in [35], the vortex energy is proportional to ρ/m. Thus, it is expected that the more favorable position for the vortex is in the less numerous component, since $\rho_i \sim N_i$. Interestingly, at confinement $f = 0.25$, there appears to be a crossover region that merits further investigation, although it falls outside the scope of this thesis.

N	N_1	N_2	f	V_i	$(E-E_{\mathrm{H.O.}})/N$ $[\hbar^2/(ma_{11}^2)]$	L $[\hbar]$	L/N_i $[\hbar]$
7.000×10^4	2.926×10^4	4.074×10^4	0.25	V_1	-9.159×10^{-6}	2.926×10^4	1.000
7.500×10^4	3.135×10^4	4.365×10^4	0.25	V_2	-9.154×10^{-6}	4.365×10^4	1.000
9.000×10^4	3.762×10^4	5.238×10^4	0.25	V_1	-0.960×10^{-5}	3.762×10^4	1.000
1.000×10^5	4.180×10^4	5.820×10^4	0.25	V_1	-0.976×10^{-5}	4.180×10^4	1.000
1.000×10^5	4.180×10^4	5.820×10^4	0.25	V_2	-0.968×10^{-5}	5.820×10^4	1.000
1.000×10^5	4.180×10^4	5.820×10^4	0.25	$\mathrm{V}_{1,2}$	-0.953×10^{-5}	1.000×10^5	1.000
1.250×10^5	5.225×10^4	7.275×10^4	0.25	V_2	-1.002×10^{-5}	7.275×10^4	1.000
2.000×10^5	8.360×10^4	1.164×10^5	0.25	V_1	-1.060×10^{-5}	8.360×10^4	1.000
3.000×10^5	1.254×10^5	1.746×10^5	0.25	V_1	-1.095×10^{-5}	1.254×10^5	1.000
1.700×10^5	7.106×10^4	0.989×10^5	0.50	V_1	-0.982×10^{-5}	7.106×10^4	1.000
1.750×10^5	7.315×10^4	1.018×10^5	0.50	V_1	-0.986×10^{-5}	7.315×10^4	1.000
1.750×10^5	7.315×10^4	1.018×10^5	0.50	V_2	-0.976×10^{-5}	1.018×10^5	1.000
2.000×10^5	8.360×10^4	1.164×10^5	0.50	V_1	-1.007×10^{-5}	8.360×10^4	1.000
2.000×10^5	8.360×10^4	1.164×10^5	0.50	V_2	-0.998×10^{-5}	1.164×10^5	1.000
2.000×10^5	8.360×10^4	1.164×10^5	0.50	$\mathrm{V}_{1,2}$	-0.984×10^{-5}	1.996×10^5	0.998
1.000×10^6	4.180×10^5	5.820×10^5	0.50	V_1	-1.158×10^{-5}	4.180×10^5	1.000
1.000×10^6	4.180×10^5	5.820×10^5	0.50	V_2	-1.161×10^{-5}	5.820×10^5	1.000
1.000×10^6	4.180×10^5	5.820×10^5	0.50	$\mathrm{V}_{1,2}$	-1.172×10^{-5}	1.000×10^6	1.000
2.400×10^5	1.003×10^5	1.397×10^5	0.75	V_1	-0.975×10^{-5}	1.003×10^5	1.000
2.750×10^5	1.150×10^5	1.600×10^5	0.75	V_2	-0.987×10^{-5}	1.600×10^5	1.000
3.000×10^5	1.254×10^5	1.746×10^5	0.75	V_1	-1.011×10^{-5}	1.254×10^5	1.000
3.000×10^5	1.254×10^5	1.746×10^5	0.75	$\mathrm{V}_{1,2}$	-0.987×10^{-5}	2.994×10^5	0.998

Table 4: *Energy per particle and angular momenta for various cases. V_i indicates that the vortex is present in component i, while N_i is the number of particles of that component. For a vortex in both $N_i = N$.*

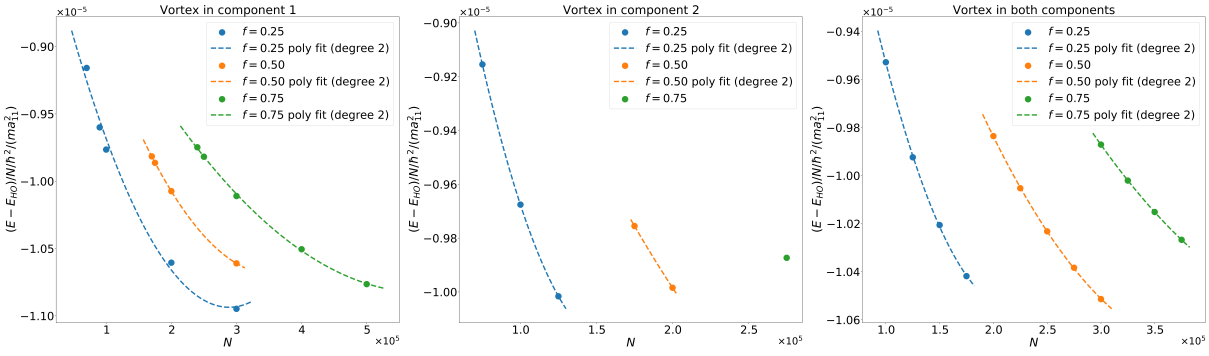

(a) **(b)** **(c)**

Figure 12: *Energy per particle for different sized droplets at different confinements with a vortex present in species 1, 2 or both. Dashed lines are a second degree polynomial fit. The fitted curves have limited validity outside the range defined by the data points.*

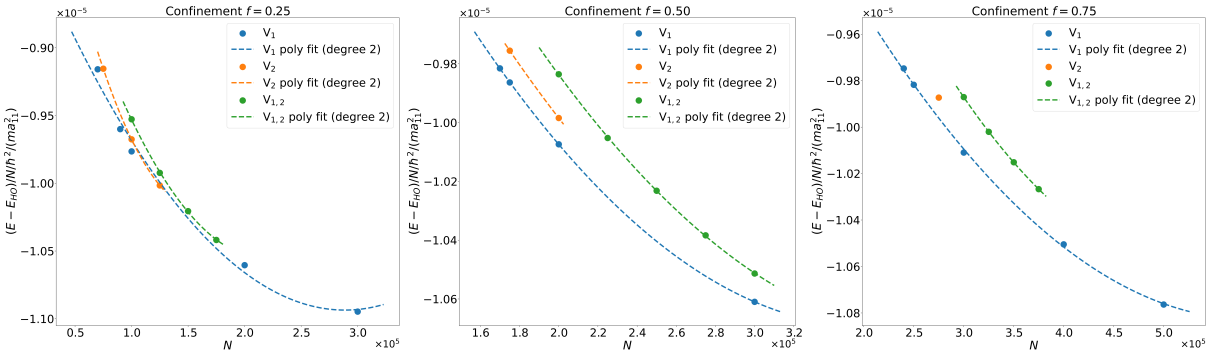

(a) **(b)** **(c)**

Figure 13: *Energy per particle for different sized droplets with a vortex V_i present in component(s) i at different confinements. Dashed lines are a second degree polynomial fit. The fitted curves have limited validity outside the range defined by the data points.*

In Figure 14, we plot the energy per particle and angular momentum per particle of the species with the vortex for a droplet containing $N = 1.75 \times 10^5$ atoms at confinement $f = 0.5$, with a vortex $l_1 = 1$ in the first species. From this, one can conclude that both the energy and angular momentum reach equilibrium values and remain stable.

Figures 15 and 16 display the total and component density cross-sections for the same droplet. In the 2D density plot in the xz-plane and the 1D section along the z-axis, the vortex line is clearly visible. In the 1D projections along the x-axis, the filling of the vortex core can be observed. When examining the densities along the z-axis, i.e., the vortex core, it is important to note that the density of the component with the vortex vanishes in accordance with theoretical predictions. As a result, the total density in the core equals the non-zero density of the vortex-free species. Even though the core is filled, the vortex-free component does not possess a flat profile but experiences a decrease in density. This is due to the vortex-free component being "dragged" by the component with the vortex, as the system tends toward the optimal density ratio $\rho_1/\rho_2 = \sqrt{a_{22}/a_{11}}$.

Figures 17 and 18 are analogous to the previous figures but depict droplets containing $N = 1 \times 10^6$ atoms. The same conclusions hold, with additional insights possible due to the larger particle number. Notably, one can observe the attainment of bulk density far from both the droplet edge and the vortex. The increase in particle number causes the droplet to expand perpendicularly to the squeezing, within the xy-plane, while maintaining the bulk density. This behavior mirrors that observed in fully vortex-free droplets. The slight slant seen in the 1D plot along the x-axis is a direct consequence of the rotation.

Figures 19 and 20 depict a droplet with $N = 1.75 \times 10^5$ atoms at confinement $f = 0.25$, with a vortex in each component. A droplet of this size cannot sustain a vortex in both species with $f = 0.50$, necessitating an increase in confinement. Increased confinement generally allows vortices to form and persist in smaller droplets, which will be discussed in more detail later.

Figure 21 illustrates the effect of squeezing on the density profile of a droplet with 3×10^5 atoms, with a vortex in species 1. At stronger squeezing (i.e., lower factor f), the density is able to develop a bulk density region. Interestingly, the squeezing does not appear to affect the size of the vortex core.

Figures 22 further showcase the effect of squeezing on the density with 2D plots. Stronger squeezing increases the droplet radius in the xy-plane while reducing its thickness in the xz-plane, as expected.

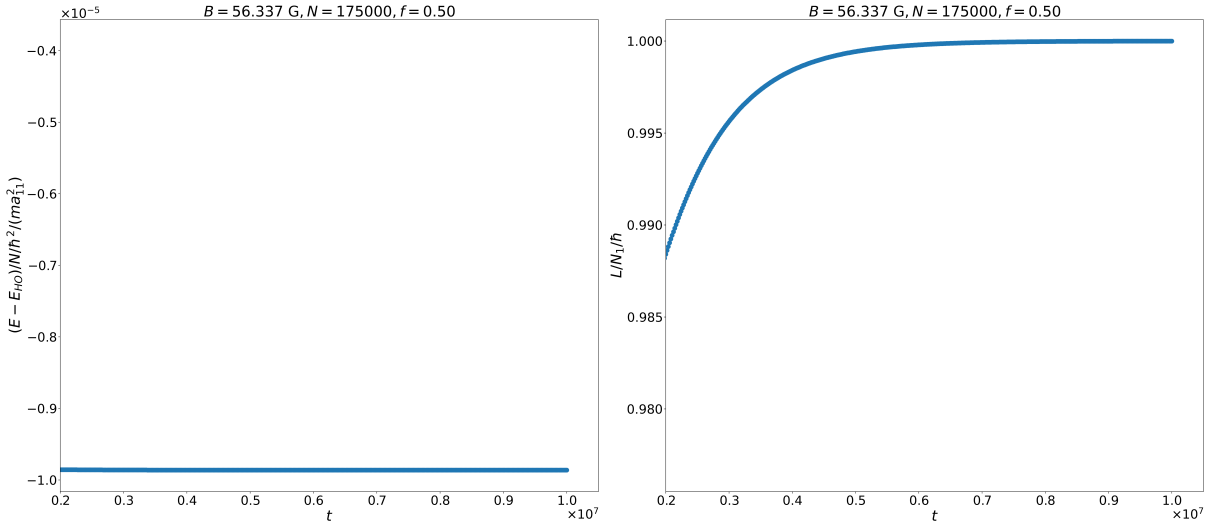

(a) *Energy per particle during the simulation.* **(b)** *Angular momentum during the simulation.*

Figure 14: *Energy and angular momentum per particle during the simulation, showing stabilization of the solution. Droplet with $N = 1.75 \times 10^5$ atoms at confinement $f = 0.5$, with a vortex in the first species, $l_1 = 1$, and no vortex in the second, $l_2 = 0$.*

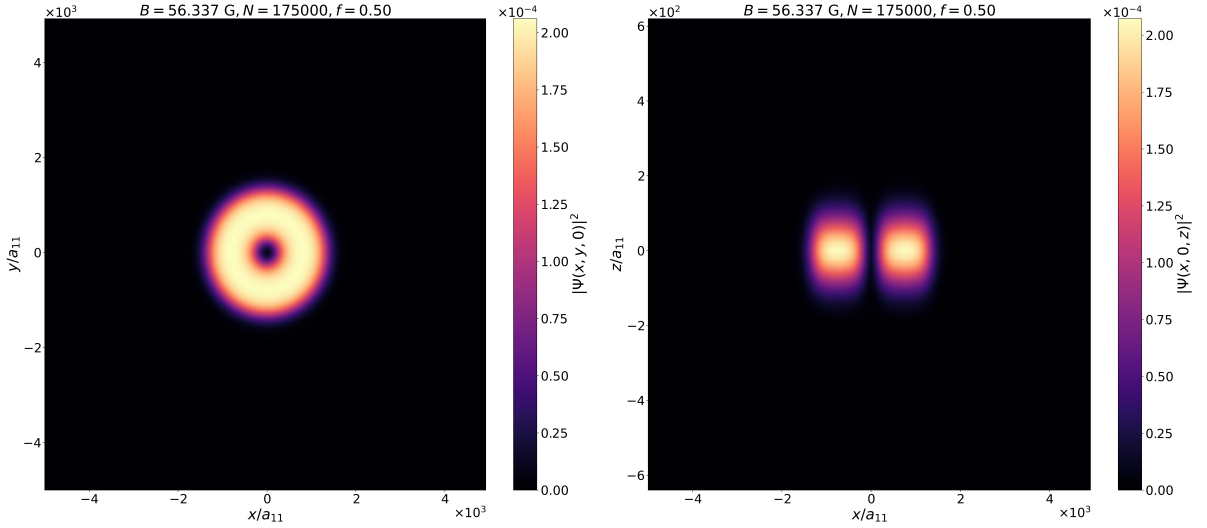

(a) *Total droplet density in the xy-plane at $z = 0$.* **(b)** *Total droplet density in the xz-plane at $y = 0$.*

Figure 15: *Total droplet density in scattering length units for a drop with $N = 1.75 \times 10^5$ atoms at confinement $f = 0.5$, with a vortex in the first species, $l_1 = 1$, and no vortex in the second, $l_2 = 0$.*

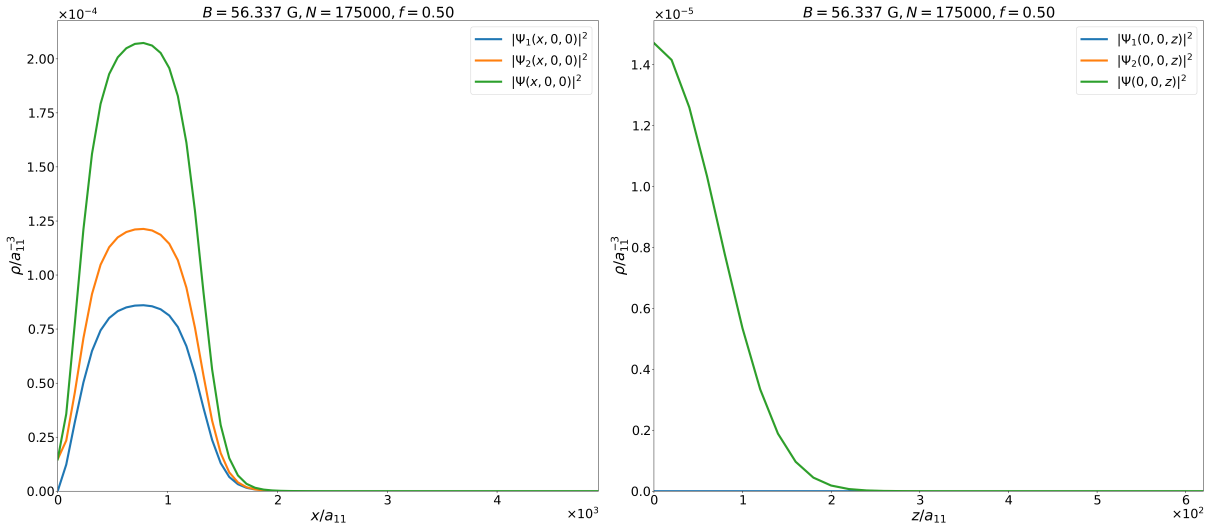

(a) *Total droplet density and component densities along the x-axis in the droplet center.*

(b) *Total droplet density and component densities along the z-axis in the droplet center. Notice that the density of the second, votrex-free, component overlaps the total density.*

Figure 16: *Component and total droplet densities in scattering length units for a drop with $N = 1.75 \times 10^5$ atoms at confinement $f = 0.5$, with a vortex in the first species, $l_1 = 1$, and no vortex in the second, $l_2 = 0$.*

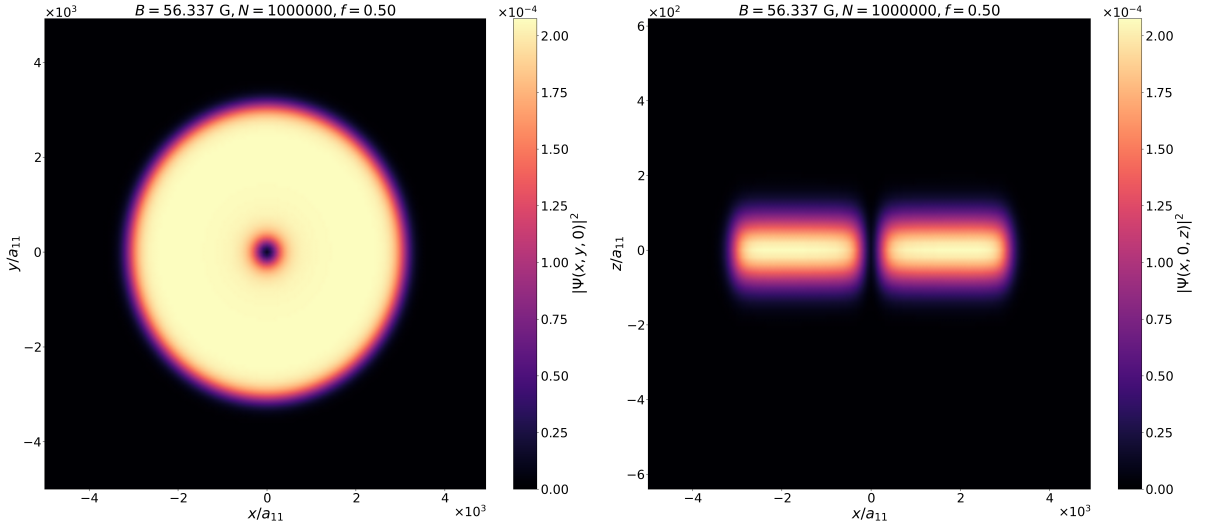

(a) *Total droplet density in the xy-plane at $z = 0$.*

(b) *Total droplet density in the xz-plane at $y = 0$.*

Figure 17: *Total droplet density in scattering length units for a drop with $N = 1 \times 10^6$ atoms at confinement $f = 0.5$, with a vortex in the first species, $l_1 = 1$, and no vortex in the second, $l_2 = 0$.*

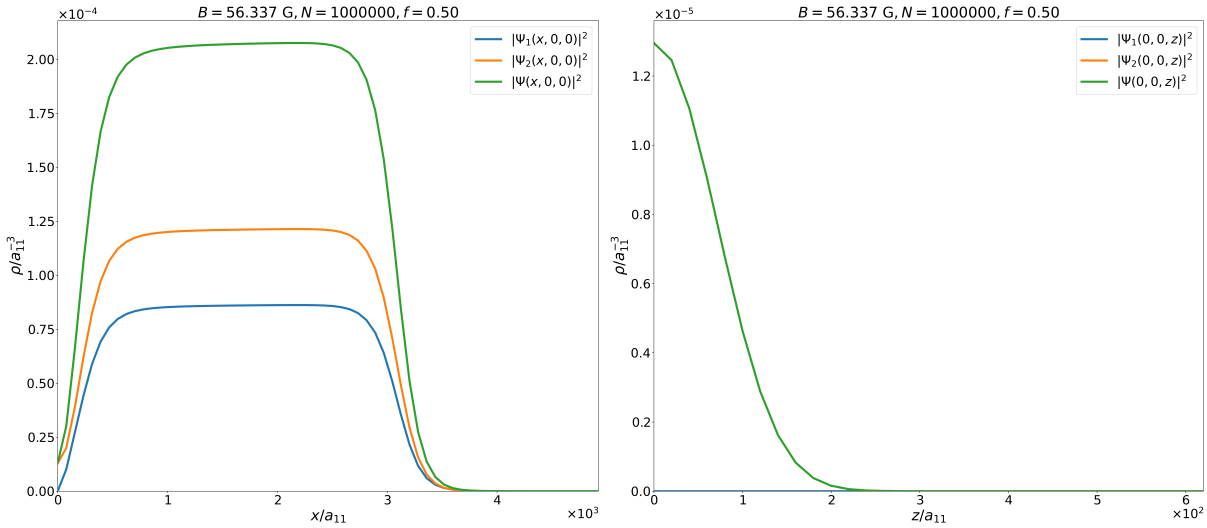

(a) *Total droplet density and component densities along the x-axis in the droplet center.*

(b) *Total droplet density and component densities along the z-axis in the droplet center. Notice that the density of the second, votrex-free, component overlaps the total density.*

Figure 18: *Component and total droplet densities in scattering length units for a drop with $N = 1 \times 10^6$ atoms at confinement $f = 0.5$, with a vortex in the first species, $l_1 = 1$, and no vortex in the second, $l_2 = 0$.*

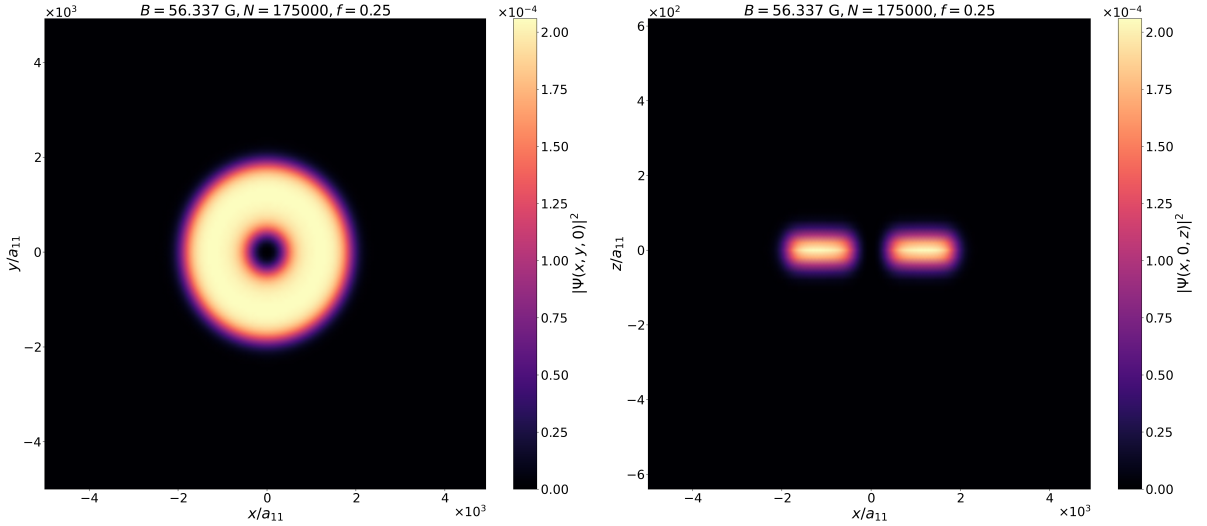

(a) *Total droplet density in the xy-plane at $z = 0$.*

(b) *Total droplet density in the xz-plane at $y = 0$.*

Figure 19: *Total droplet density in scattering length units for a drop with $N = 1.75 \times 10^5$ atoms at confinement $f = 0.25$, with a vortex in both components, $l_1 = 1$, $l_2 = 1$.*

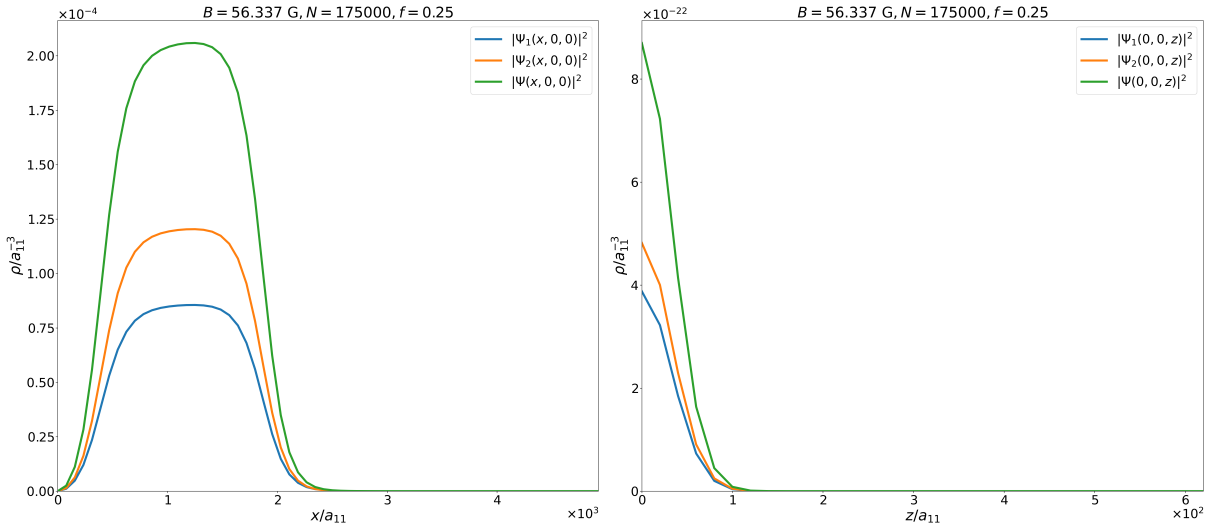

(a) *Total droplet density and component densities along the x-axis in the droplet center.*

(b) *Total droplet density and component densities along the z-axis in the droplet center. Notice that the densities both components are within numerical uncertanties zero (check order of magnitude).*

Figure 20: *Component and total droplet densities in scattering length units for a drop with $N = 1.75 \times 10^5$ atoms at confinement $f = 0.25$, with a a vortex in both components, $l_1 = 1$, $l_2 = 1$.*

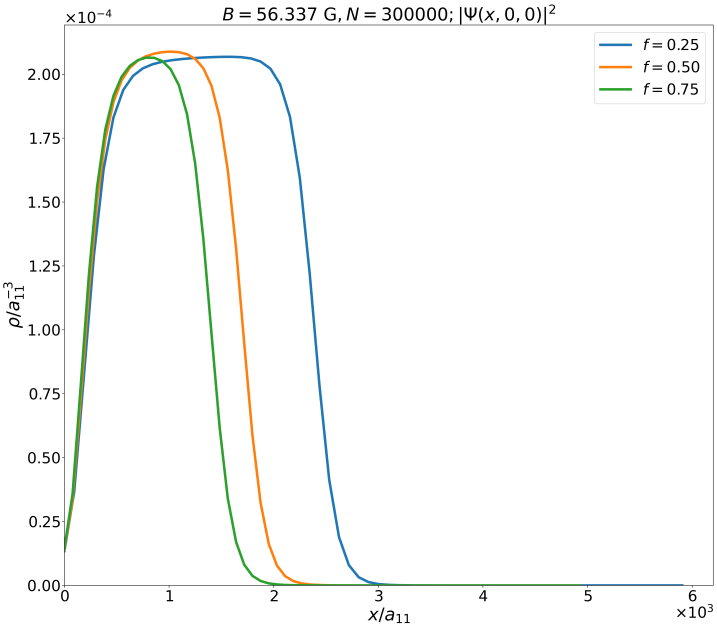

Figure 21: *Effect of squeezing on the total droplet density along the x-axis in the droplet center. Droplet with $N = 3 \times 10^5$ at three confinements, $f = 0.25, 0.50, 0.75$, with a vortex in the first species, $l_1 = 1$, and no vortex in the second, $l_2 = 0$.*

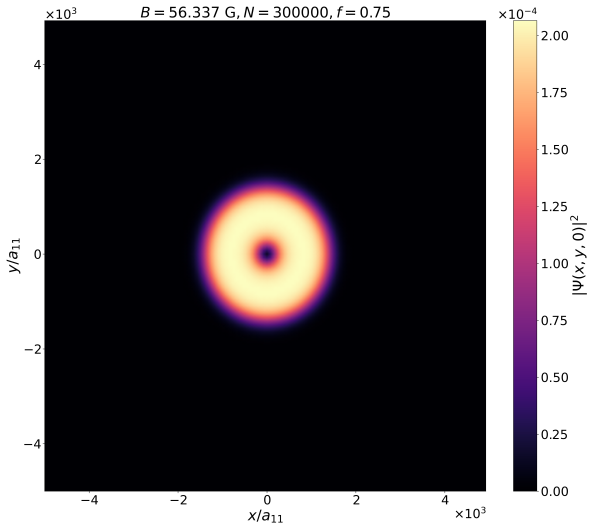

(a) *Total droplet density in the xy-plane at $z = 0$.*

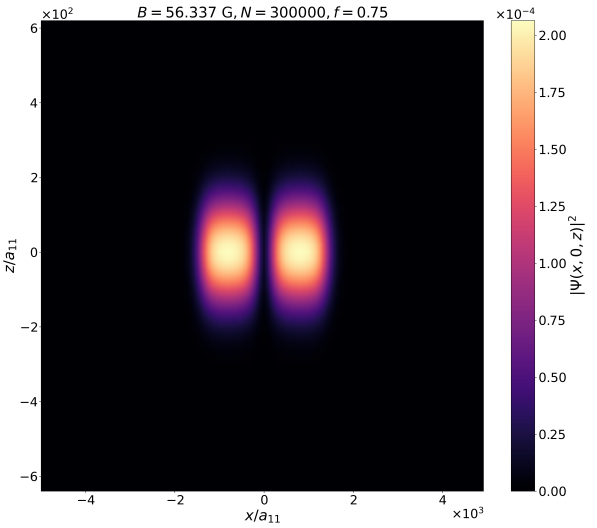

(b) *Total droplet density in the xz-plane at $y = 0$.*

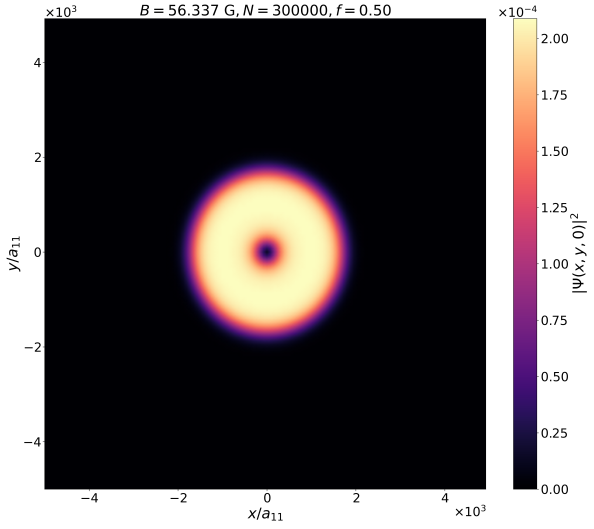

(c) *Total droplet density in the xy-plane at $z = 0$.*

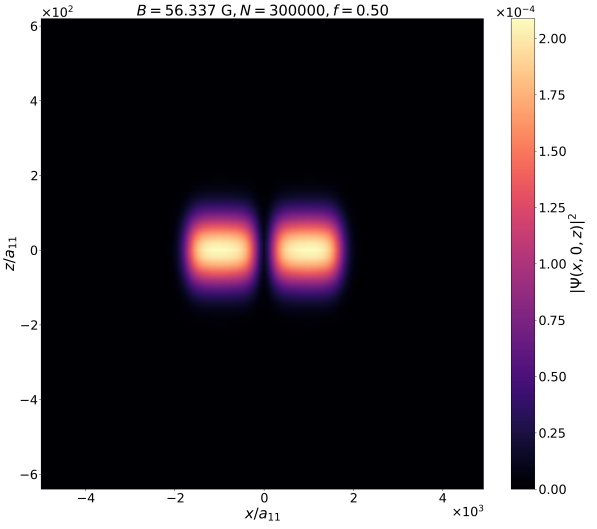

(d) *Total droplet density in the xz-plane at $y = 0$.*

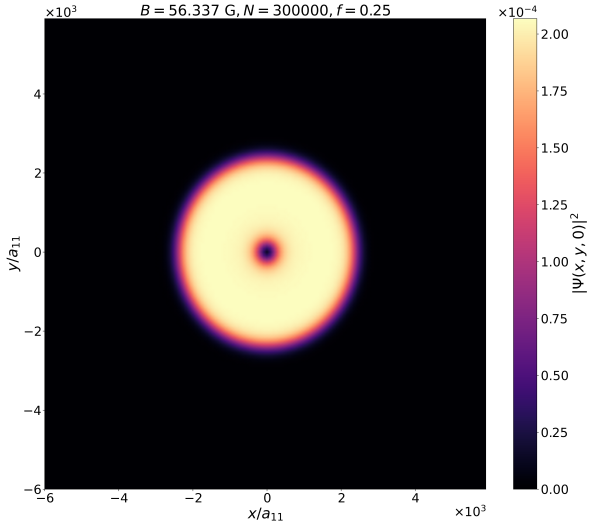

(e) *Total droplet density in the xy-plane at $z = 0$.*

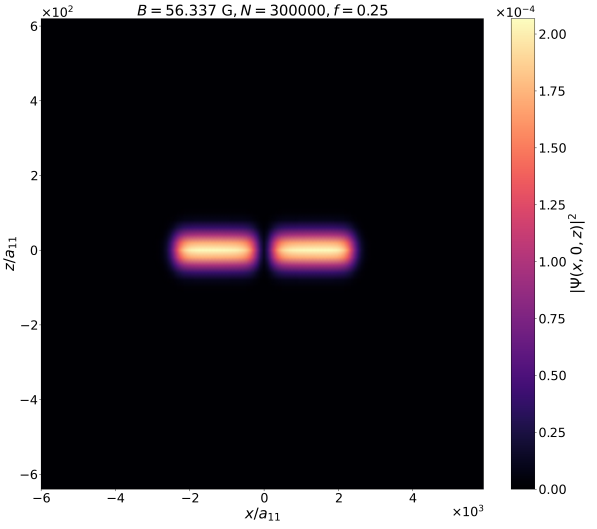

(f) *Total droplet density in the xz-plane at $y = 0$.*

Figure 22: *Effect of squeezing on the total droplet density in the xy- and xz-planes. Droplet with $N = 3 \times 10^5$ at various confinements, with a vortex in the first species, $l_1 = 1$, and no vortex in the second, $l_2 = 0$. The size of the simulation box is slightly larger in the case of strongest squeezing, $f = 0.25$.*

7.3 Critical atom number for vortex hosting

The critical atom number typically refers to the minimum number of atoms required for a droplet to be self-bound. This concept is particularly useful in experiments, as working with smaller droplets — i.e., with fewer atoms — is generally more practical. While all the droplets considered in this thesis are self-bound, not all of them can sustain a vortex. There is a minimum number of atoms required for a vortex state to be a stable ground state, which we denote as the *critical atom number* $N_{\mathrm{c,\,v}}$. Table 5 presents our findings. Contrary to what the extrapolation of the fits in Figures 12 and 13 might suggest, droplets do not exhibit stable vortex states for arbitrarily low numbers of atoms.

The stability of vortices was tested with size increments of 10^4 atoms for a vortex in the less numerous species 1, and 2.5×10^4 atoms for a vortex in species 2 or vortices in both species. Based on the binding energy results, it was expected that vortices could be sustained in smaller droplets when present in the less numerous species, species 1. Our findings confirm this expectation. The critical atom number is slightly lower for a vortex in species 1 compared to a vortex in species 2. Achieving a stable vortex in both components requires the largest number of atoms, though this number is still less than the sum of the critical numbers for each individual species.

Furthermore, when examining different confinements, it was observed that as the droplet becomes more squeezed, fewer atoms are required to sustain a vortex. This result is intuitive, as increased squeezing not only brings the system closer to a quasi-2D configuration, but also strengthens the self-binding of the droplet. Consequently, such systems become easier to realize experimentally.

Figure 23 illustrates the angular momentum per atom of the vortex component at squeezing $f = 0.50$, with a vortex in species 2, close to the edge of vortex stability and the case of vortex expulsion, which may lead to the droplet's breakup. When $N < N_{\mathrm{c,\,v}}$, the angular momentum rapidly converges to zero, indicating the instability of the vortex state.

Confinement factor	$f = 0.25$	$f = 0.50$	$f = 0.75$
Vortex in 1	7.00×10^4	1.70×10^5	2.40×10^5
Vortex in 2	7.50×10^4	1.75×10^5	2.75×10^5
Vortex in both	1.0×10^5	2.00×10^5	3.00×10^5

Table 5: *Critical atom number $N_{c,\,v}$ for vortex states at different confinements f.*

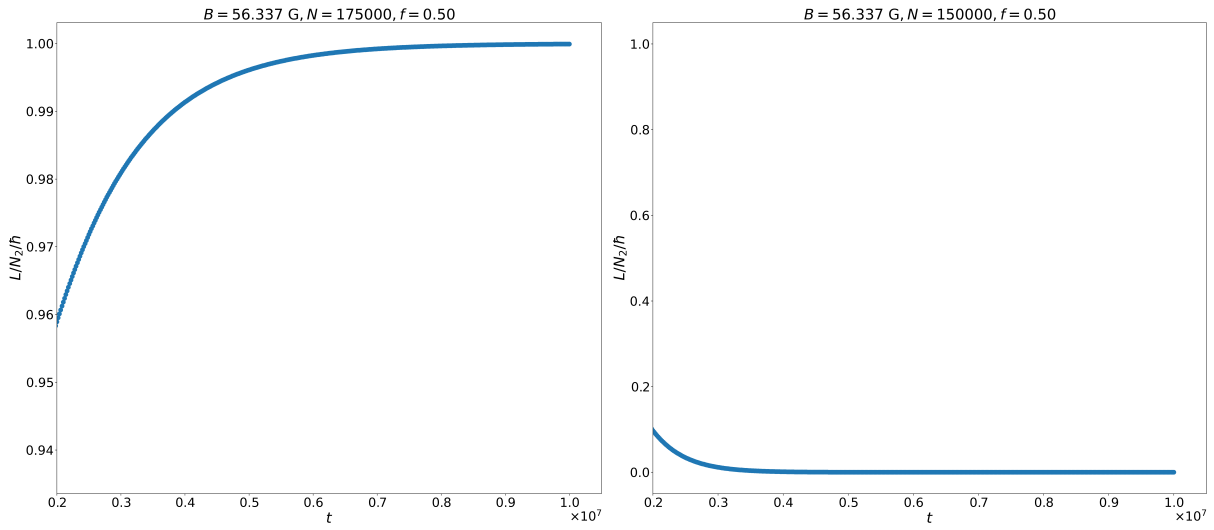

(a) *Simulation near the critical atom number. Number of atoms in the droplet is* $N = 1.75 \times 10^5$.

(b) *Simulation below the critical atom number. Number of atoms in the droplet is* $N = 1.50 \times 10^5$.

Figure 23: *Angular momentum per particle of the species with the vortex during the simulation, showing stabilization of the solution and vortex expulsion. Droplet confined at* $f = 0.5$*, with no vortex in the first species* $l_1 = 0$ *and a vortex of charge* $l_2 = 1$ *in the second species.*

7.4 Larger quantization vortex

Higher quantization vortices are generally less energetically favorable. This can be understood from equation (4.23), which shows that the energy depends on l^2 (denoted as s^2 in the equation). This implies that it is more favorable to have two vortices of quantum number $l = 1$ rather than a single vortex with $l = 2$. Figure 24 compares the density profiles for a droplet with $N = 1 \times 10^6$ atoms at confinement $f = 0.25$, featuring an $l = 1$ vortex in the first species and an $l = 2$ vortex in either species.

Interestingly, droplets with an $l = 2$ vortex do not break down as might be expected. The emergence of $l = 2$ vortices warrants further and more time-consuming investigation to confirm the results, including smaller time steps and finer discretization. If the large vortex breaks down into two smaller vortices, they wouldn't be centered, but rather offset. This posits the question of whether there is space to facilitate such configurations. The stability of the $l = 2$ vortex might be a finite-size effect that would disappear for a larger droplet.

Another noteworthy observation is that in the presence of an $l = 2$ vortex, there seems to be minimal vortex core filling, while the droplet radius remains roughly the same. However, the vortex core radius is significantly larger. Figures 25 and 26 display the 2D and 1D density profiles, respectively. We observe that the vortex core filling is present but two orders of magnitude smaller than that of $l = 1$ vortices (Figure 18).

Table 6 summarizes the energies, revealing that the higher quanta vortex state appears to be

more self-bound. This observation requires further investigation. One possibility is that the state is metastable and, under real-world conditions, would quickly break down. A first step in further research would be to test this solution in real-time simulations and assess its robustness against small perturbations. Angular momentum behaves in accordance with expectations, reaching a value of $2\hbar$ per particle of the component with the vortex.

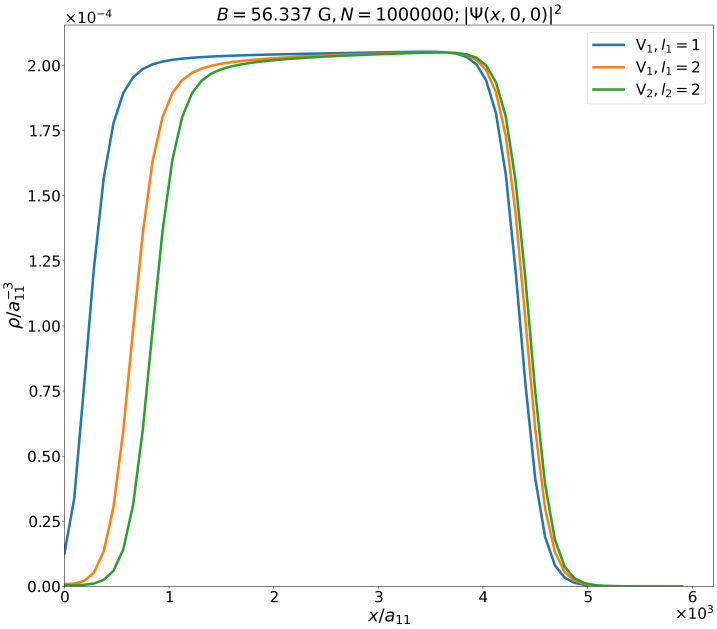

Figure 24: *Comparison of the total droplet density along the x-axis in the droplet center. Droplet with $N = 1 \times 10^6$ atoms at confinement $f = 0.25$, with a $l_1 = 1$ vortex in the first species and cases of $l = 2$ vortex in the first or second species.*

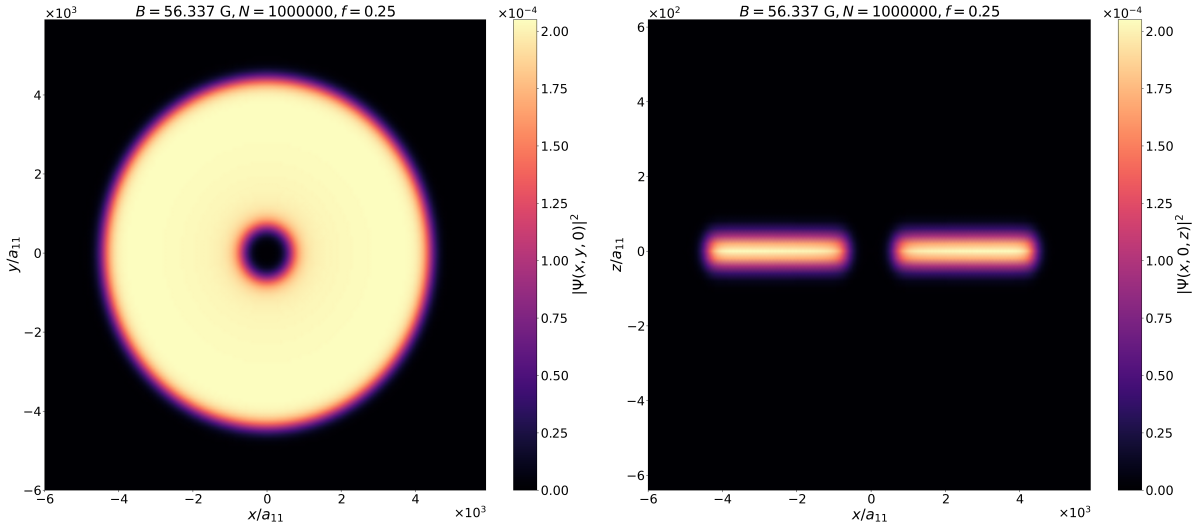

(a) *Total droplet density in the xy-plane at $z = 0$.* **(b)** *Total droplet density in the xz-plane at $y = 0$.*

Figure 25: *Total droplet density in scattering length units for a drop with $N = 1 \times 10^6$ atoms at confinement $f = 0.25$, with a higher quanta vortex in the first species, $l_1 = 2$, and no vortex in the second, $l_2 = 0$.*

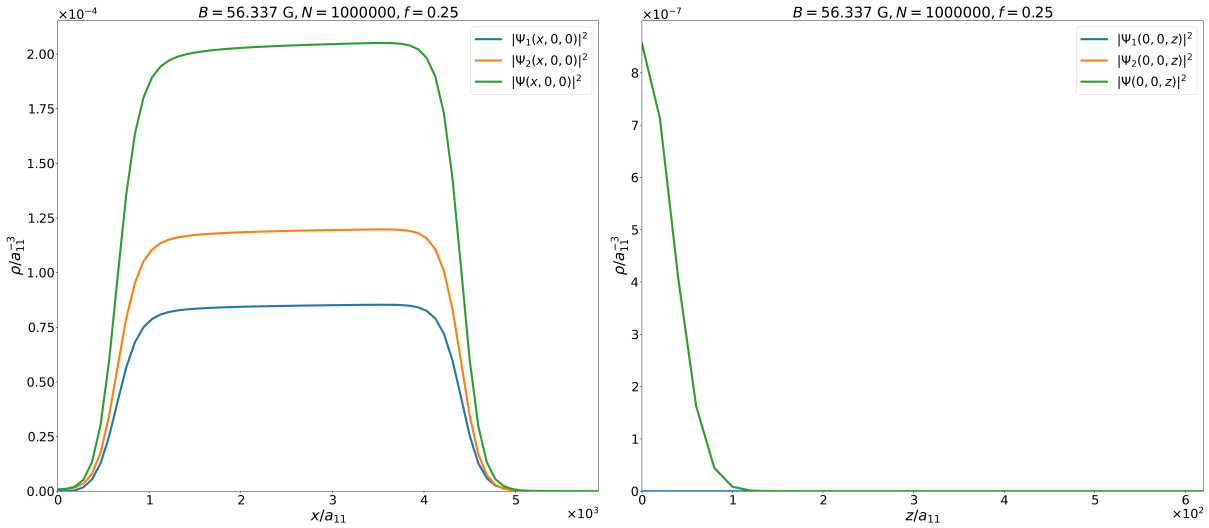

(a) *Total droplet density and component densities along the x-axis in the droplet center.*

(b) *Total droplet density and component densities along the z-axis in the droplet center. Notice that the density of the second, votrex-free, component overlaps the total density.*

Figure 26: *Component and total droplet densities in scattering length units for a drop with $N = 1 \times 10^6$ atoms at confinement $f = 0.25$, with a higher quanta vortex in the first species, $l_1 = 2$, and no vortex in the second, $l_2 = 0$.*

N	N_1	N_2	f	V_i	$(E - E_{\mathrm{H.O.}})/N$ $[\hbar^2/(ma_{11}^2)]$	L $[\hbar]$	L/N_i $[\hbar]$
1.000×10^6	4.180×10^5	5.820×10^5	0.25	V_1, $l_1 = 1$	-1.157×10^{-5}	4.180×10^5	1.000
1.000×10^6	4.180×10^5	5.820×10^5	0.25	V_1, $l_1 = 2$	-1.162×10^{-5}	8.360×10^5	2.000
1.000×10^6	4.180×10^5	5.820×10^5	0.25	V_2, $l_2 = 2$	-1.172×10^{-5}	1.164×10^6	2.000

Table 6: *Energy per particle and angular momenta for a droplet with $N = 1 \times 10^6$ atoms at confinement $f = 0.25$, with a $l_1 = 1$ vortex in the first species and cases of $l = 2$ vortex in the first or second species. V_i indicates that the vortex is present in component i, while N_i is the number of particles of that component.*

8 Conclusion

This thesis investigated quantum droplets composed of two hyperfine states of potassium-39, confined along one axis. The interactions were modeled using Density Functional Theory (DFT) to account for both mean-field and Lee-Huang-Yang (LHY) contributions. The extended Gross-Pitaevskii equation in the rotating frame was solved in imaginary time to perform the calculations.

For non-rotating vortex-free droplets, the density profiles and energies were consistent with previous calculations conducted using different methods. As demonstrated in that earlier research [34], stronger squeezing results in a larger droplet area perpendicular to the squeezing axis and a smaller one along it. Additionally, increasing the number of atoms causes the droplet to expand perpendicularly to the squeezing, while maintaining bulk density.

We also explored various methods for calculating angular momentum. The computationally fastest approach was found to be the use of Fast Fourier Transforms (FFT), which maintains a level of accuracy comparable to that of directly implementing $\hat{L}_z$ using numerical differentiation with fourth-order accuracy $O(h^4)$.

When examining droplets with vortices, it was observed that placing a vortex in the less numerous component of the mixture results in a more strongly bound droplet. In contrast, the droplet is least bound when a vortex is present in both species, as expected. Stronger squeezing leads to more strongly bound droplets. The angular momentum per atom in the species with the vortex is $1\hbar$, consistent with theoretical predictions. Vortex core filling by the vortex-free species was observed, in line with expectations and previous studies [42, 47].

The critical number of atoms required for vortex stability was determined with precision of 10^4 for the vortex in the less numerous, energetically favourable species, and 2.5×10^4 for other configurations. Consistent with expectations, a vortex can be sustained in the less numerous component in smaller droplets. Higher confinement makes it easier to sustain a vortex, potentially bringing such systems within the reach of experimental research.

Interestingly, vortices with larger quantization appear to be stable and more self-bound. However, this result warrants further investigation, as it may be an artifact of the numerical method used for the chosen parameters. It is possible that this vortex would break down if real time propagation were used, rather than imaginary.

Overall, our findings suggest several potential avenues for future research. Refining this approach in more confined quasi-2D systems could provide experimentally feasible setups for studying vortices in self-bound quantum droplets, due to the increased stability of vortices in highly confined systems. This would not only facilitate the exploration of vortex arrays but also open up the potential for studying vortex-antivortex pairs with quantum numbers ± 1. Another avenue would be to further study the current setup, extending the consideration to real time

propagation. The controlled creation and manipulation of vortices in droplets could be utilized to simulate complex quantum systems or to develop new sensing techniques based on the precise control of quantum states.

Additionally, vortices of higher quanta might be attainable in squeezed quantum droplets; however, this requires further research to eliminate the possibility of a numerical artifact.

9 Bibliography

[1] A. Einstein. Quantum theory of the monatomic ideal gas. Part I and Part II. Sitzungsber. Preuss. Akad. Wiss., 1:3–14, 1925.

[2] S. N. Bose. Plancks Gesetz und Lichtquantenhypothese. Zeitschrift für Physik, 26: 178–181, 1924.

[3] H. Kamerlingh Onnes. Further experiments with liquid helium. C. On the change of electric resistance of pure metals at very low temperatures etc. IV. The resistance of pure mercury at helium temperatures. Commun. Phys. Lab. Univ. Leiden, 120b:1274–1276, 1911.

[4] P. Kapitza. Viscosity of liquid helium below the λ-point. Nature, 141:74–75, 1938. doi: 10.1038/141074a0. URL https://doi.org/10.1038/141074a0.

[5] J. F. Allen and D. Misener. Flow of liquid helium II. Nature, 141:75, 1938. doi: 10.1038/141075a0. URL https://doi.org/10.1038/141075a0.

[6] F. London. The λ-Phenomenon of Liquid Helium and the Bose-Einstein Degeneracy. Nature, 141:643–644, 1938. doi: doi.org/10.1038/141643a0. URL https://doi.org/10.1038/141643a0.

[7] L. Tisza. Transport Phenomena in Helium II. Nature, 141:913–914, 1938. doi: 10.1038/141913a0. URL https://doi.org/10.1038/141913a0.

[8] L. Landau. Theory of the Superfluidity of Helium II. Phys. Rev., 60:356–358, Aug 1941. doi: 10.1103/PhysRev.60.356. URL https://link.aps.org/doi/10.1103/PhysRev.60.356.

[9] N. N. Bogoliubov. On the theory of superfluidity. Journal of Physics, 11:23–32, 1947.

[10] L. D. Landau and E. M. Lifshitz. Statisticheskai Fizika. Fizmatgiz, Moscow, 1951.

[11] O. Penrose. CXXXVI. On the quantum mechanics of helium II. The London, Edinburgh, and Dublin Philosophical Magazine and Journal of Science, 42(335):1373–1377, 1951. doi: 10.1080/14786445108560954. URL https://doi.org/10.1080/14786445108560954.

[12] Oliver Penrose and Lars Onsager. Bose-Einstein Condensation and Liquid Helium. Phys. Rev., 104:576–584, Nov 1956. doi: 10.1103/PhysRev.104.576. URL https://link.aps.org/doi/10.1103/PhysRev.104.576.

[13] Lars Onsager. Statistical Hydrodynamics. Il Nuovo Cimento (1943-1954), 6(Suppl 2): 279–287, 1949.

[14] R.P. Feynman. Chapter II Application of Quantum Mechanics to Liquid Helium. Progress in Low Temperature Physics, 1:17–53, 1955. ISSN 0079-6417. doi: https://doi.org/10.1016/S0079-6417(08)60077-3. URL https://www.sciencedirect.com/science/article/pii/S0079641708600773.

[15] H. E. Hall and W. F. Vinen. The Rotation of Liquid Helium II: I. Experiments on the Propagation of Second Sound in Uniformly Rotating Helium II. Proc. Roy. Soc. Lond. A, 238:204–214, 1956. URL http://doi.org/10.1098/rspa.1956.0214.

[16] T. D. Lee, Kerson Huang, and C. N. Yang. Eigenvalues and Eigenfunctions of a Bose System of Hard Spheres and Its Low-Temperature Properties. Phys. Rev., 106: 1135–1145, Jun 1957. doi: 10.1103/PhysRev.106.1135. URL https://link.aps.org/doi/10.1103/PhysRev.106.1135.

[17] Theodore H. Maiman. Stimulated Optical Radiation in Ruby. Nature, 187:493–494, 1960. URL https://doi.org/10.1038/187493a0.

[18] E. L. Raab, M. Prentiss, Alex Cable, Steven Chu, and D. E. Pritchard. Trapping of Neutral Sodium Atoms with Radiation Pressure. Phys. Rev. Lett., 59:2631–2634, Dec 1987. doi: 10.1103/PhysRevLett.59.2631. URL https://link.aps.org/doi/10.1103/PhysRevLett.59.2631.

[19] M. H. Anderson, J. R. Ensher, M. R. Matthews, C. E. Wieman, and E. A. Cornell. Observation of Bose-Einstein Condensation in a Dilute Atomic Vapor. Science, 269 (5221):198–201, 1995. doi: 10.1126/science.269.5221.198. URL https://www.science.org/doi/abs/10.1126/science.269.5221.198.

[20] K. B. Davis, M. O. Mewes, M. R. Andrews, N. J. van Druten, D. S. Durfee, D. M. Kurn, and W. Ketterle. Bose-Einstein Condensation in a Gas of Sodium Atoms. Phys. Rev. Lett., 75:3969–3973, Nov 1995. doi: 10.1103/PhysRevLett.75.3969. URL https://link.aps.org/doi/10.1103/PhysRevLett.75.3969.

[21] E. A. Cornell and C. E. Wieman. Nobel Lecture: Bose-Einstein condensation in a dilute gas, the first 70 years and some recent experiments. Rev. Mod. Phys., 74:875–893, Aug 2002. doi: 10.1103/RevModPhys.74.875. URL https://link.aps.org/doi/10.1103/RevModPhys.74.875.

[22] D. S. Petrov. Quantum Mechanical Stabilization of a Collapsing Bose-Bose Mixture. Phys. Rev. Lett., 115:155302, Oct 2015. doi: 10.1103/PhysRevLett.115.155302. URL https://link.aps.org/doi/10.1103/PhysRevLett.115.155302.

[23] C. R. Cabrera, L. Tanzi, J. Sanz, B. Naylor, P. Thomas, P. Cheiney, and L. Tarruell. Quantum liquid droplets in a mixture of Bose-Einstein condensates. Science, 359(6373):

301–304, 2018. doi: 10.1126/science.aao5686. URL https://www.science.org/doi/abs/10.1126/science.aao5686.

[24] G. Semeghini, G. Ferioli, L. Masi, C. Mazzinghi, L. Wolswijk, F. Minardi, M. Modugno, G. Modugno, M. Inguscio, and M. Fattori. Self-Bound Quantum Droplets of Atomic Mixtures in Free Space. Phys. Rev. Lett., 120:235301, Jun 2018. doi: 10.1103/PhysRevLett.120.235301. URL https://link.aps.org/doi/10.1103/PhysRevLett.120.235301.

[25] Russell J. Donnelly and Carlo F. Barenghi. The Observed Properties of Liquid Helium at the Saturated Vapor Pressure. Journal of Physical and Chemical Reference Data, 27(6): 1217–1274, 11 1998. ISSN 0047-2689. doi: 10.1063/1.556028. URL https://doi.org/10.1063/1.556028.

[26] D.R. Lide. CRC Handbook of Chemistry and Physics, 85th Edition. Number s. 85 in CRC Handbook of Chemistry and Physics, 85th Ed. Taylor & Francis, 2004. ISBN 9780849304859. URL https://books.google.hr/books?id=WDll8hA006AC.

[27] Cheng Chin, Rudolf Grimm, Paul Julienne, and Eite Tiesinga. Feshbach resonances in ultracold gases. Rev. Mod. Phys., 82:1225–1286, Apr 2010. doi: 10.1103/RevModPhys.82.1225. URL https://link.aps.org/doi/10.1103/RevModPhys.82.1225.

[28] Igor Ferrier-Barbut, Holger Kadau, Matthias Schmitt, Matthias Wenzel, and Tilman Pfau. Observation of Quantum Droplets in a Strongly Dipolar Bose Gas. Phys. Rev. Lett., 116: 215301, May 2016. doi: 10.1103/PhysRevLett.116.215301. URL https://link.aps.org/doi/10.1103/PhysRevLett.116.215301.

[29] Matthias Schmitt, Matthias Wenzel, Fabian Böttcher, Igor Ferrier-Barbut, and Tilman Pfau. Self-bound droplets of a dilute magnetic quantum liquid. Nature, 539(7628): 259–262, November 2016. ISSN 1476-4687. doi: 10.1038/nature20126. URL http://doi.org/10.1038/nature20126.

[30] D. Baillie, R. M. Wilson, R. N. Bisset, and P. B. Blakie. Self-bound dipolar droplet: A localized matter wave in free space. Phys. Rev. A, 94:021602, Aug 2016. doi: 10.1103/PhysRevA.94.021602. URL https://link.aps.org/doi/10.1103/PhysRevA.94.021602.

[31] Fabian Böttcher, Jan-Niklas Schmidt, Matthias Wenzel, Jens Hertkorn, Mingyang Guo, Tim Langen, and Tilman Pfau. Transient Supersolid Properties in an Array of Dipolar Quantum Droplets. Phys. Rev. X, 9:011051, Mar 2019. doi: 10.1103/PhysRevX.9.011051. URL https://link.aps.org/doi/10.1103/PhysRevX.9.011051.

[32] C. D'Errico, A. Burchianti, M. Prevedelli, L. Salasnich, F. Ancilotto, M. Modugno, F. Minardi, and C. Fort. Observation of quantum droplets in a heteronuclear bosonic mixture. Phys. Rev. Res., 1:033155, Dec 2019. doi: 10.1103/PhysRevResearch.1.033155. URL https://link.aps.org/doi/10.1103/PhysRevResearch.1.033155.

[33] Zhichao Guo, Fan Jia, Lintao Li, Yinfeng Ma, Jeremy M. Hutson, Xiaoling Cui, and Dajun Wang. Lee-Huang-Yang effects in the ultracold mixture of ^{23}Na and ^{87}Rb with attractive interspecies interactions. Phys. Rev. Res., 3:033247, Sep 2021. doi: 10.1103/PhysRevResearch.3.033247. URL https://link.aps.org/doi/10.1103/PhysRevResearch.3.033247.

[34] A. Sanuy, R. Barač, P. Stipanović, L. Vranje š Markić, and J. Boronat. Squeezing Bose-Bose liquid drops, Jan 2024. URL https://link.aps.org/doi/10.1103/PhysRevA.109.013313.

[35] Matteo Caldara and Francesco Ancilotto. Vortices in quantum droplets of heteronuclear Bose mixtures. Phys. Rev. A, 105:063328, Jun 2022. doi: 10.1103/PhysRevA.105.063328. URL https://link.aps.org/doi/10.1103/PhysRevA.105.063328.

[36] Lev Pitaevskii and Sandro Stringari. Bose-Einstein Condensation and Superfluidity. Oxford University Press, 01 2016. ISBN 9780198758884. doi: 10.1093/acprof:oso/9780198758884.001.0001. URL https://doi.org/10.1093/acprof:oso/9780198758884.001.0001.

[37] C. J. Pethick and H. Smith. Bose-Einstein Condensation in Dilute Gases. Cambridge University Press, Cambridge, UK, 2nd edition, 2008. ISBN 978-0521846516.

[38] R.K. Pathria and P.D. Beale. Statistical Mechanics. Elsevier Science, 2011. ISBN 9780123821898. URL https://books.google.hr/books?id=KdbJJAXQ-RsC.

[39] E. P. Gross. Structure of a quantized vortex in boson systems. Nuovo Cimento, 20: 454–477, 1961. doi: 10.1007/BF02731494. URL https://doi.org/10.1007/BF02731494.

[40] L. Pitaevskii. Vortex lines in an imperfect Bose gas. Soviet Physics JETP, 13:451–454, 1961. Translated from ZhETF.

[41] Viktor Cikojević. Ab-initio Quantum Monte Carlo study of ultracold atomic mixtures, 2021. URL https://arxiv.org/abs/2105.01439.

[42] Francesco Ancilotto, Manuel Barranco, Montserrat Guilleumas, and Martí Pi. Self-bound ultradilute Bose mixtures within local density approximation. Phys. Rev. A, 98:053623,

Nov 2018. doi: 10.1103/PhysRevA.98.053623. URL https://link.aps.org/doi/10.1103/PhysRevA.98.053623.

[43] D. M. Larsen. Binary Mixtures of Dilute Bose Gases with Repulsive Interactions at Zero Temperature. Annals of Physics, 24(3):89–101, 1963. doi: https://doi.org/10.1016/0003-4916(63)90066-6. URL https://www.sciencedirect.com/science/article/pii/0003491663900666.

[44] L.D. Landau and E.M. Lifshitz. Fluid Mechanics: Landau and Lifshitz: Course of Theoretical Physics, Volume 6. Elsevier Science, 2013. ISBN 9781483161044. URL https://books.google.hr/books?id=eOBbAwAAQBAJ.

[45] Siu A. Chin and Eckhard Krotscheck. Fourth-order algorithms for solving the imaginary-time Gross-Pitaevskii equation in a rotating anisotropic trap. Phys. Rev. E, 72: 036705, Sep 2005. doi: 10.1103/PhysRevE.72.036705. URL https://link.aps.org/doi/10.1103/PhysRevE.72.036705.

[46] M. Ö. Oktel. Vortex lattice of a Bose-Einstein condensate in a rotating anisotropic trap. Phys. Rev. A, 69:023618, Feb 2004. doi: 10.1103/PhysRevA.69.023618. URL https://link.aps.org/doi/10.1103/PhysRevA.69.023618.

[47] Matteo Caldara. Angular momentum and shapes of rotating quantum droplets. Master's thesis, University of Padua, Padua, Italy, 2021. URL https://hdl.handle.net/20.500.12608/21500. Physics, Scuola di Scienze.